Impact of the Brink-Axel hypothesis on unique first-forbidden *β*-transitions for *r*-process nuclei*

Fakeha Farooq[1] Jameel-Un Nabi[2] Ramoona Shehzadi[1†]

[1]Department of Physics, University of the Punjab, Quaid-e-Azam Campus 54590, Lahore, Pakistan
[2]University of Wah, Quaid Avenue, Wah Cantt 47040, Punjab, Pakistan

Abstract: Key nuclear inputs for the astrophysical *r*-process simulations are the weak interaction rates. Consequently, the accuracy of these inputs directly affects the reliability of nucleosynthesis modeling. The majority of the stellar rates, used in simulation studies are calculated by invoking the Brink-Axel (BA) hypothesis. The BA hypothesis assumes that the strength functions of all parent excited states are the same as for the ground state, only shifted in energies. However, the BA hypothesis has to be tested against microscopically calculated state-by-state rates. In this project, we study the impact of the BA hypothesis on calculated stellar β^--decay and electron capture rates. Our investigation include both unique first forbidden (U1F) and allowed transitions for 106 neutron-rich trans-iron nuclei ([27, 77] ≤ [*Z*, *A*] ≤ [82, 208]). The calculations were performed using the deformed proton-neutron quasiparticle random-phase approximation (*pn*-QRPA) model with a simple plus quadrupole separable and schematic interaction. Waiting-point and several key *r*-process nuclei lie within the considered mass region of the nuclear chart. We computed electron capture and β^--decay rates using two different prescriptions for strength functions. One was based on invoking the BA hypothesis and the other was the state-by-state calculation of strength functions, under stellar density and temperature conditions ($[10, 1] \leq [\rho Y_e(\mathrm{g/cm^3}), T(GK)] \leq [10^{11}, 30]$). Our results show that the BA hypothesis invoked U1F β^- rates are overestimated by 4–5 orders of magnitude as compared to microscopic rates. For capture rates, more than two orders of magnitude differences were noted when applying the BA hypothesis. It was concluded that the BA hypothesis is not a reliable approximation, especially for β^--decay forbidden transitions.

Keywords: Brink-Axel hypothesis, *pn*-QRPA model, unique first forbidden *β*-transitions, GT strength functions, trans-iron nuclei, *r*-process

DOI: 10.1088/1674-1137/ad1925

I. INTRODUCTION

In astrophysical measures, forbidden transitions are the key elements to study the weak nuclear processes ($\beta^\pm$-decays and electron captures), in addition to the allowed transitions [1–4]. When the electron chemical potential of the stellar interior approaches ~30 [MeV], first-forbidden (FF) transitions become important relative to the allowed Gamow-Teller (GT) rates. The β^--decay half-lives of nuclei having large *Z* numbers and with *Z* and *N* beyond closed shells have sizable contributions from FF decays [5, 6]. Reliable calculation of weak rates, including β^--decay (BD) and electron capture (EC), on heavy trans-iron neutron-rich nuclei ($70 \leq A \leq 208$) are a prerequisite to studying the rapid neutron-capture (*r*-) process [7–9]. Particularly, the weak rates associated with FF BD transitions on closed-shell waiting-point (WP) nuclei, with N numbers 50, 82, and 126, can potentially affect the progression of matter in the *r*-process pathway. The observed peaks in the abundance pattern of *r*-process elements arise due to the deceleration of matter flow at these WPs. Thus, matter assembles at the WP, and nuclei undergo a series of BDs before the *r*-process recommences [2, 10–16]. The high temperature (> 1 GK) and high neutron density (> 10^{20} g/cm^3) conditions associated with the neutron-star to neutron-star collisions [17] and core-collapse supernovae (CCSNe)[11] establish a site for creating the *r*-process elements.

The weak rates are calculated based on charge-changing strength functions or transition probabilities. The charge-exchange reactions provide GT strength distribution data from the ground states of high mass nuclei (*e.g.*, [18–23]). However, measurements can provide information only for a limited number of nuclei. In addition, in an

Received 14 October 2023; Accepted 28 December 2023; Published online 29 December 2023
* J.-U. Nabi is supported by the Higher Education Commission Pakistan through Project (0-15394/NRPU/R&D/HEC/2021)
† E-mail: ramoona.physics@pu.edu.pk

exotic stellar environment, states can be thermally populated, and transitions from the excited states, which generally are not measurable under lab conditions, contribute significantly [7, 24]. Despite the improved measurement facilities on new heavy-ion accelerators (*e.g.*, [25–29]), obtaining satisfactory and accurate information from high-lying excited states using experiments seems daunting. Consequently, astrophysical simulations rely heavily on theoretical estimations. However, it is still challenging for nuclear models to perform rate calculations near neutron (proton) drip lines and regions of higher mass nuclei, owing to the complex structures of correlated many-body nuclear systems. The majority of the previously calculated set of weak rate calculations [24, 30–33] used an approximate method invoking the so-called Brink-Axel (BA) hypothesis [34, 35]. Several studies have investigated the accuracy of the BA hypothesis [36–47]. Most of these works have shown that the BA hypothesis is a poor approximation for usage in calculations related to stellar weak rates. The test of the effectiveness of the BA hypothesis is crucial for reliable estimation of stellar weak rates. To the best of our knowledge, earlier studies did not cover the *r*-process nuclei nor the validity of the BA hypothesis for computing forbidden transitions. The present investigation reports the effectiveness of the BA hypothesis for calculating the stellar (EC and BD) weak rate. We selected 106 *r*-process nuclei ($27 \le Z \le 82$ and $70 \le A \le 208$) and studied their allowed and U1F transitions under stellar conditions. The calculation of terrestrial BD half-lives and β-delayed neutron-emission probabilities of the nuclei has remained the focus of many past investigations. These include experimental [25–27, 29, 48] and theoretical studies based on the shell model [3, 32, 49], QRPA +Gross theory [2], density functional + continuum QRPA [16, 50], empirical calculations [51], machine learning [52], relativistic Hatree-Bogoliubov + QRPA [15], *pn*-QRPA [53, 54], and relativistic QRPA [55].

The current manuscript is structured as follows. Section II briefly describes the *pn*-QRPA formalism calculating the strength functions and decay rates for the U1F and allowed (GT) transitions. The results are discussed in Sec. III. Finally, Sec. IV highlights the findings of the current investigation.

II. THEORETICAL FORMALISM

A simple and microscopic theoretical framework based on the *pn*-QRPA theory was employed to check the reliability of the BA hypothesis for weak rate calculations, including U1F and allowed GT transitions. Using a separable and schematic interaction made access to up to 7 major oscillatory shells model space possible in the current calculation. This enabled us to calculate strength functions in a state-by-state fashion for high-mass nuclei considered in this project. This simple yet effective microscopic approach has wide applications in astrophysical studies [4, 6, 56, 57].

The *pn*-QRPA theory deals with the quasiparticle states of proton-neutron systems and correlations between them. The ground state is a vacuum for the QRPA phonon, $\hat{\Gamma}_\omega|\mathrm{QRPA}\rangle = 0$, with the phonon creation operator defined by

$$\hat{\Gamma}^{\dagger}_{\omega}(\mu) = \sum_{\pi,\nu} X^{\pi\nu}_{\omega}(\mu)\hat{a}^{\dagger}_{\pi}\hat{a}^{\dagger}_{\bar{\nu}} - Y^{\pi\nu}_{\omega}(\mu)\hat{a}_{\nu}\hat{a}_{\bar{\pi}}, \tag{1}$$

where ν and π, respectively, denote the neutron and proton single quasiparticle states, and $(\hat{a}^{\dagger},\hat{a})$ are the creation and annihilation operators of these states. The sum runs over all possible $\pi\nu$-pairs which satisfy $\mu = m_\pi - m_\nu$, with $m_\pi(m_\nu)$ being the third component of angular momentum. The forward-going (X_ω) and backward-going (Y_ω) amplitudes and energy (ω) are the eigenvectors and eigenvalues, respectively, of the famous (Q)RPA equation

$$\begin{bmatrix} M & N \\ -N & -M \end{bmatrix}\begin{bmatrix} X \\ Y \end{bmatrix} = \omega \begin{bmatrix} X \\ Y \end{bmatrix}. \tag{2}$$

The solution of the RPA equation (Eq. (2)) was obtained for each projection value ($\mu = 0, \pm 1$ for allowed and $\mu = 0, \pm 1, \pm 2$ for U1F transitions). The M and N matrix elements are given by

$$\begin{aligned} M_{\pi\nu,\pi'\nu'} =& \delta_{\pi\nu,\pi'\nu'}(\varepsilon_\pi + \varepsilon_\nu) \\ &+ V^{\mathrm{pp}}_{\pi\nu,\pi'\nu'}(v_\pi v_\nu v_{\pi'} v_{\nu'} + u_\pi u_\nu u_{\pi'} u_{\nu'}) \\ &+ V^{\mathrm{ph}}_{\pi\nu,\pi'\nu'}(v_\pi u_\nu v_{\pi'} u_{\nu'} + u_\pi v_\nu u_{\pi'} v_{\nu'}), \end{aligned} \tag{3}$$

$$\begin{aligned} N_{\pi\nu,\pi'\nu'} =& V^{\mathrm{pp}}_{\pi\nu,\pi'\nu'}(u_\pi u_\nu v_{\pi'} v_{\nu'} + v_\pi v_\nu u_{\pi'} u_{\nu'}) \\ &- V^{\mathrm{ph}}_{\pi\nu,\pi'\nu'}(v_\pi u_\nu u_{\pi'} v_{\nu'} + u_\pi v_\nu v_{\pi'} u_{\nu'}), \end{aligned} \tag{4}$$

where the quasiparticle energies $(\varepsilon_\pi, \varepsilon_\nu)$ and the occupation amplitudes $(u_{\pi(\nu)}, v_{\pi(\nu)})$, which satisfy $u^2 + v^2 = 1$, were obtained from the BCS calculations. In the first step, the quasiparticle basis was constructed in terms of nucleon states and defined by Bogoliubov transformation with pairing correlations. Later, in the quasiparticle proton-neutron pairs, the computation of the RPA equation (Eq. (2)) was performed with separable GT residual forces, namely particle-hole (ph) and particle-particle (pp) forces. We took the pp GT force as [58]

$$\hat{V}_{\mathrm{pp(GT)}} = -2\kappa_{\mathrm{GT}} \sum_{\mu} (-1)^{\mu} \hat{P}^{\dagger}_{\mu} \hat{P}_{-\mu}, \tag{5}$$

where

$$\hat{P}_{\mu}^{\dagger} = \sum_{j_\pi m_\pi j_\nu m_\nu} \langle j_\nu m_\nu | (\sigma_\mu \tau_-)^{\dagger} | j_\pi m_\pi \rangle (-1)^{l_\nu + j_\nu - m_\nu} \hat{c}^{\dagger}_{j_\pi m_\pi} \hat{c}^{\dagger}_{j_\nu - m_\nu}, \quad (6)$$

and the ph GT force is [59]

$$\hat{V}_{\mathrm{ph(GT)}} = 2\chi_{GT} \sum_{\mu} (-1)^{\mu} \hat{R}_{\mu} \hat{R}^{\dagger}_{-\mu}, \quad (7)$$

where

$$\hat{R}_{\mu} = \sum_{j_\pi m_\pi j_\nu m_\nu} \langle j_\pi m_\pi | \sigma_\mu \tau_- | j_\nu m_\nu \rangle \hat{c}^{\dagger}_{j_\pi m_\pi} \hat{c}_{j_\nu m_\nu}. \quad (8)$$

Introducing positive values of force constants ($\chi_{\mathrm{GT}}, \kappa_{\mathrm{GT}}$), ensured the attractive and repulsive nature of the pp and ph GT forces, respectively. Using the separable GT forces in the calculation, the RPA matrix equation is reduced to a 4$^{\mathrm{th}}$ order algebraic equation. The method to determine the roots of these equations can be seen in [60]. This saves the computational time relative to the full diagonalization of the nuclear Hamiltonian.

In the RPA formalism, excitations from the ground state ($J^{\pi} = 0^{+}$) of an even-even nucleus are considered. The ground-state of an odd-odd (odd-A) parent nucleus is expressed as a proton-neutron quasiparticle pair (one quasiparticle) state of the smallest energy. Then, the two possible transitions are the phonon excitations (in which quasiparticle merely plays the role of a spectator) and the transition of the quasiparticle. In the latter case, correlations of phonon to the quasiparticle transitions were treated in first-order perturbation [61, 62]. Next, we present quasiparticle transitions, construction of phonon-related multi-quasiparticle states (representing nuclear excited levels of even-even, odd-A, and odd-odd nuclei) and formulae of GT transitions within the current model using the recipe given by [60]. The phonon-correlated one quasiparticle states are defined by

$$|\pi_{\mathrm{corr}}\rangle = a^{\dagger}_{\pi}|-\rangle + \sum_{\nu,\omega} a^{\dagger}_{\nu} A^{\dagger}_{\omega}(\mu)|-\rangle \langle -|[a^{\dagger}_{\nu} A^{\dagger}_{\omega}(\mu)]^{\dagger} H_{31} a^{\dagger}_{\pi}|-\rangle \times E_{\pi}(\nu,\omega), \quad (9)$$

$$|\nu_{\mathrm{corr}}\rangle = a^{\dagger}_{\nu}|-\rangle + \sum_{\pi,\omega} a^{\dagger}_{\pi} A^{\dagger}_{\omega}(-\mu)|-\rangle \langle -|[a^{\dagger}_{\pi} A^{\dagger}_{\omega}(-\mu)]^{\dagger} H_{31} a^{\dagger}_{\nu}|-\rangle \times E_{\nu}(\pi,\omega), \quad (10)$$

with

$$E_a(b,\omega) = \frac{1}{\epsilon_a - \epsilon_b - \omega}, \qquad a,b = \pi,\nu, \quad (11)$$

where the terms $E_a(b,\omega)$ can be modified to prevent the singularity in the transition amplitude caused by the first-order perturbation of the odd-particle wave function. The first term in Eq. (9) and Eq. (10) denotes the proton (neutron) quasiparticle state, while the second term denotes RPA correlated phonons admixed with quasiparticle phonon coupled Hamiltonian H_{31}, which was accomplished by Bogoliubov transformation from separable pp and ph GT interaction forces. The summation applies to all phonon states and neutron (proton) quasiparticle states, satisfying $m_\pi - m_\nu = \mu$ with $\pi_\pi \pi_\nu = 1$. The calculation of the quasiparticle transition amplitudes for correlated states can be seen in [63]. The amplitudes of GT transitions in terms of separable forces are

$$\begin{aligned} <\pi_{\mathrm{corr}}|\tau_-\sigma_\mu|\nu_{\mathrm{corr}}> =& q^{U}_{\pi\nu} + 2\chi_{GT}[q^{U}_{\pi\nu} \sum_{\omega} (Z^{-2}_{\omega} E_{\pi}(\nu,\omega) + Z^{+2}_{\omega} E_{\nu}(\pi,\omega)) \\ &- q^{V}_{\pi\nu} \sum_{\omega} Z^{-}_{\omega} Z^{+}_{\omega} (E_{\pi}(\nu,\omega) + E_{\nu}(\pi,\omega))] + 2\kappa_{GT}[q_{\pi\nu} \sum_{\omega} (Z^{-}_{\omega} Z^{-}_{\omega} E_{\pi}(\nu,\omega) - Z^{+}_{\omega} Z^{++}_{\omega} E_{\nu}(\pi,\omega)) \\ &- \tilde{q}_{\pi\nu} \sum_{\omega} (Z^{-}_{\omega} Z^{++}_{\omega} E_{\pi}(\nu,\omega) - Z^{+}_{\omega} Z^{-}_{\omega} E_{\nu}(\pi,\omega))], \end{aligned} \quad (12)$$

$$\begin{aligned} <\pi_{\mathrm{corr}}|\tau_+\sigma_\mu|\nu_{\mathrm{corr}}> =& q^{V}_{\pi\nu} + 2\chi_{GT}[q^{V}_{\pi\nu} \sum_{\omega} (Z^{+2}_{\omega} E_{\pi}(\nu,\omega) + Z^{-2}_{\omega} E_{\nu}(\pi,\omega)) \\ &- q^{U}_{\pi\nu} \sum_{\omega} Z^{-}_{\omega} Z^{+}_{\omega} (E_{\pi}(\nu,\omega) + E_{\nu}(\pi,\omega))] + 2\kappa_{GT}[\tilde{q}_{\pi\nu} \sum_{\omega} (Z^{+}_{\omega} Z^{++}_{\omega} E_{\pi}(\nu,\omega) - Z^{-}_{\omega} Z^{-}_{\omega} E_{\nu}(\pi,\omega)) \\ &- q_{\pi\nu} \sum_{\omega} (Z^{+}_{\omega} Z^{-}_{\omega} E_{\pi}(\nu,\omega) - Z^{-}_{\omega} Z^{++}_{\omega} E_{\nu}(\pi,\omega))], \end{aligned} \quad (13)$$

$$<\nu_{\mathrm{corr}}|\tau_{\pm}\sigma_{-\mu}|\pi_{\mathrm{corr}}> = (-1)^{\mu} <\pi_{\mathrm{corr}}|\tau_{\mp}\sigma_{\mu}|\nu_{\mathrm{corr}}> . \quad (14)$$

In Eqs. (12), (13), and (14), σ_μ and $\tau_\pm$ are spin and iso-spin type operators, respectively, and the other symbols $q_{\pi\nu}$ ($\tilde{q}_{\pi\nu}$), $q^U_{\pi\nu}$ ($q^V_{\pi\nu}$), Z^-_ω (Z^+_ω) and Z^-_ω (Z^{++}_ω) are defined as

$$
\begin{aligned}
&q_{\pi\nu} = f_{\pi\nu}u_\pi v_\nu, \quad q^U_{\pi\nu} = f_{\pi\nu}u_\pi u_\nu,\\
&\tilde{q}_{\pi\nu} = f_{\pi\nu}v_\pi u_\nu, \quad {}^V_{\pi\nu} = f_{\pi\nu}v_\pi v_\nu\\
&Z^-_\omega = \sum_{\pi,\nu}(X^{\pi\nu}_\omega q_{\pi\nu} - Y^{\pi\nu}_\omega \tilde{q}_{\pi\nu}),\\
&Z^+_\omega = \sum_{\pi,\nu}(X^{\pi\nu}_\omega \tilde{q}_{\pi\nu} - Y^{\pi\nu}_\omega q_{\pi\nu}),\\
&Z^-_\omega = \sum_{\pi,\nu}(X^{\pi\nu}_\omega q^U_{\pi\nu} + Y^{\pi\nu}_\omega q^V_{\pi\nu}),\\
&Z^{++}_\omega = \sum_{\pi\nu}(X^{\pi,\nu}_\omega q^V_{\pi\nu} + Y^{\pi\nu}_\omega q^U_{\pi\nu}).
\end{aligned} \tag{15}
$$

The terms $X^{\pi\nu}_\omega$ and $Y^{\pi\nu}_\omega$ were defined earlier, and other symbols have usual meanings. The idea of quasiparticle transitions with first-order phonon correlations can be extended to an odd-odd parent nucleus. The ground state is assumed to be a proton-neutron quasiparticle pair state of the smallest energy. The GT transitions of the quasiparticle lead to two-proton or two-neutron quasiparticle states in the even-even daughter nucleus. The two quasiparticle states were constructed with phonon correlations and given by

$$
\begin{aligned}
|\pi\nu_{\rm corr}> &= a^\dagger_\pi a^\dagger_\nu|-> + \frac{1}{2}\sum_{\pi'_1,\pi'_2,\omega} a^\dagger_{\pi'_1}a^\dagger_{\pi'_2}A^\dagger_\omega(-\mu)|->\\
&\times <-|[a^\dagger_{\pi'_1}a^\dagger_{\pi'_2}A^\dagger_\omega(-\mu)]^\dagger H_{31}a^\dagger_\pi a^\dagger_\nu|-> E_{\pi\nu}(\pi'_1\pi'_2,\omega)\\
&+\frac{1}{2}\sum_{\nu'_1,\nu'_2,\omega} a^\dagger_{\nu'_1}a_{\nu'_2}A^\dagger_\omega(\mu)|->\\
&\times <-|[a^\dagger_{\nu'_1}a^\dagger_{\nu'_2}A^\dagger_\omega(\mu)]^\dagger H_{31}a^\dagger_\pi a^\dagger_\nu|-> E_{\pi\nu}(\nu'_1\nu'_2,\omega),
\end{aligned} \tag{16}
$$

$$
\begin{aligned}
<\pi_1\pi_{2{\rm corr}}| &= a^\dagger_{\pi_1}a^\dagger_{\pi_2}|-> + \sum_{\pi',\nu',\omega} a^\dagger_{\pi'}a^\dagger_{\nu'}A^\dagger_\omega(\mu)|->\\
&\times <-|[a^\dagger_{\pi'}a^\dagger_{\nu'}A^\dagger_\omega(\mu)]^\dagger H_{31}a^\dagger_{\pi_1}a^\dagger_{\pi_2}|->\\
&\times E_{\pi_1\pi_2}(\pi'\nu',\omega),
\end{aligned} \tag{17}
$$

$$
\begin{aligned}
<\nu_1\nu_{2{\rm corr}}| &= a^\dagger_{\nu_1}a^\dagger_{\nu_2}|-> + \sum_{\pi',\nu',\omega} a^+_{\pi'}a^\dagger_{\nu'}A^\dagger_\omega(-\mu)|->\\
&\times <-|[a^\dagger_{\pi'}a^\dagger_{\nu'}A^\dagger_\omega(-\mu)]^\dagger H_{31}a^\dagger_{\nu_1}a^\dagger_{\nu_2}|->\\
&\times E_{\nu_1\nu_2}(\pi'\nu',\omega),
\end{aligned} \tag{18}
$$

where,

$$
E_{ab}(cd,\omega) = \frac{1}{(\epsilon_a+\epsilon_b)-(\epsilon_c+\epsilon_d+\omega)} \tag{19}
$$

where subscript index a (b) denotes π, π_1, and ν_1 (ν, π_2 and ν_2), and c (d) denotes π', π'_1, and ν'_1 (ν', π'_2 and ν'_2). The GT transition amplitudes between these states were reduced to those of one quasiparticle states

$$
\begin{aligned}
&<\pi_1\pi_{2{\rm corr}}|\tau_\pm\sigma_\mu|\pi\nu_{\rm corr}>\\
&=\delta(\pi_1,\pi) <\pi_{2{\rm corr}}|\tau_\pm\sigma_\mu|\nu_{\rm corr}>\\
&\quad-\delta(\pi_2,\pi) <\pi_{1{\rm corr}}|\tau_\pm\sigma_\mu|\nu_{\rm corr}>,
\end{aligned} \tag{20}
$$

$$
\begin{aligned}
&<\nu_1\nu_{2{\rm corr}}|\tau_\pm\sigma_{-\mu}|\pi\nu_{\rm corr}>\\
&=\delta(\nu_2,\nu) <\nu_{1{\rm corr}}|\tau_\pm\sigma_{-\mu}|\pi_{\rm corr}>\\
&\quad-\delta(\nu_1,\nu) <\nu_{2{\rm corr}}|\tau_\pm\sigma_{-\mu}|\pi_{\rm corr}>,
\end{aligned} \tag{21}
$$

by ignoring the terms of second order in the correlated phonons. QRPA phonon excitations are also possible for the odd-odd parent nuclei, where the quasiparticle pair acts as spectators in the same single quasiparticle shells. The nuclear excited states can be constructed as phonon correlated multi quasiparticle states. The transition amplitudes between the multi quasiparticle states can be reduced to those of one quasiparticle states, as described below.

The excited levels of an even-even nucleus are the two-proton and two-neutron quasiparticle states. Transitions from these initial states to final neutron-proton quasiparticle pair states are possible in the odd-odd daughter nuclei. The transition amplitudes can be reduced to correlated quasiparticle states by taking the Hermitian conjugate of Eqs. (20) and (21)

$$
\begin{aligned}
&<\pi\nu_{\rm corr}|\tau_\pm\sigma_{-\mu}|\pi_1\pi_{2{\rm corr}}>\\
&= -\delta(\pi,\pi_2) <\nu_{\rm corr}|\tau_\pm\sigma_{-\mu}|\pi_{1{\rm corr}}>\\
&\quad+\delta(\pi,\pi_1) <\nu_{\rm corr}|\tau_\pm\sigma_{-\mu}|\pi_{2{\rm corr}}>,
\end{aligned} \tag{22}
$$

$$
\begin{aligned}
&<\pi\nu_{\rm corr}|\tau_\pm\sigma_\mu|\nu_1\nu_{2{\rm corr}}>\\
&=\delta(\nu,\nu_2) <\pi_{\rm corr}|\tau_\pm\sigma_\mu|\nu_{1{\rm corr}}>\\
&\quad-\delta(\nu,\nu_1) <\pi_{\rm corr}|\tau_\pm\sigma_\mu|\nu_{2{\rm corr}}>.
\end{aligned} \tag{23}
$$

When a nucleus has an odd nucleon (a proton and/or a neutron), low-lying states are obtained by lifting the quasiparticle in the orbit of the smallest energy to higher-lying orbits. States of an odd-proton even-neutron nucleus were expressed by three-proton states or one proton two-neutron states, corresponding to the excitation of a proton or neutron

$$|\pi_1\pi_2\pi_{3\mathrm{corr}}\rangle = a^\dagger_{\pi_1}a^\dagger_{\pi_2}a^\dagger_{\pi_3}|-\rangle + \frac{1}{2}\sum_{\pi_1',\pi_2',\nu',\omega} a^\dagger_{\pi_1'}a^\dagger_{\pi_2'}a^\dagger_{\nu'}A^\dagger_\omega(\mu)|-\rangle \times\langle -|[a^\dagger_{\pi_1'}a^\dagger_{\pi_2'}a^\dagger_{\nu'}A^\dagger_\omega(\mu)]^\dagger H_{31}a^\dagger_{\pi_1}a^\dagger_{\pi_2}a^\dagger_{\pi_3}|-\rangle \times E_{\pi_1\pi_2\pi_3}(\pi_1'\pi_2'\nu',\omega), \tag{24}$$

$$|\pi_1\nu_1\nu_{2\mathrm{corr}}\rangle = a^\dagger_{\pi_1}a^\dagger_{\nu_1}a^\dagger_{\nu_2}|-\rangle + \frac{1}{2}\sum_{\pi_1',\pi_2',\nu',\omega} a^\dagger_{\pi_1'}a^\dagger_{\pi_2'}a^\dagger_{\nu'}A^\dagger_\omega(-\mu)|-\rangle \times\langle -|[a^\dagger_{\pi_1'}a^\dagger_{\pi_2'}a^\dagger_{\nu'}A^\dagger_\omega(-\mu)]^\dagger H_{31}a^\dagger_{\pi_1}a^\dagger_{\nu_1}a^\dagger_{\nu_2}|-\rangle \times E_{\pi_1\nu_1\nu_2}(\pi_1'\pi_2'\nu',\omega) + \frac{1}{6}\sum_{\nu_1',\nu_2',\nu_3',\omega} a^\dagger_{\nu_1'}a^\dagger_{\nu_2'}a^\dagger_{\nu_3'}A^\dagger_\omega(\mu)|-\rangle \times\langle -|[a^\dagger_{\nu_1'}a^\dagger_{\nu_2'}a^\dagger_{\nu_3'}A^\dagger_\omega(\mu)]^\dagger H_{31}a^\dagger_{\pi_1}a^\dagger_{\nu_1}a^\dagger_{\nu_2}|-\rangle \times E_{\pi_1\nu_1\nu_2}(\nu_1'\nu_2'\nu_3',\omega), \tag{25}$$

with the energy denominators of first order perturbation,

$$E_{abc}(\mathrm{def},\omega) = \frac{1}{(\epsilon_a+\epsilon_b+\epsilon_c-\epsilon_d-\epsilon_e-\epsilon_f-\omega)}, \tag{26}$$

where the subscripts represent π_1, π_2, π_3, ν_1, and ν_2 (π_1', π_2', ν', ν_1', ν_2' and ν_2'). These equations can be used to generate the three quasiparticle states of odd-proton and even-neutron by swapping the neutron and proton states, $\nu\longleftrightarrow\pi$ and $A^\dagger_\omega(\mu)\longleftrightarrow A^\dagger_\omega(-\mu)$. The amplitudes of the quasiparticle transitions between the three quasiparticle states were reduced to those for correlated one quasiparticle states. For parent nuclei with an odd proton,

$$\langle\pi_1'\pi_2'\nu'_{1\mathrm{corr}}|\tau_\pm\sigma_{-\mu}|\pi_1\pi_2\pi_{3\mathrm{corr}}\rangle = \delta(\pi_1',\pi_2)\delta(\pi_2',\pi_3)\langle\nu'_{1\mathrm{corr}}|\tau_\pm\sigma_{-\mu}|\pi_{1\mathrm{corr}}\rangle - \delta(\pi_1',\pi_1)\delta(\pi_2',\pi_3)\langle\nu'_{1\mathrm{corr}}|\tau_\pm\sigma_{-\mu}|\pi_{2\mathrm{corr}}\rangle + \delta(\pi_1',\pi_1)\delta(\pi_2',\pi_2)\langle\nu'_{1\mathrm{corr}}|\tau_\pm\sigma_{-\mu}|\pi_{3\mathrm{corr}}\rangle, \tag{27}$$

$$\langle\pi_1'\pi_2'\nu'_{1\mathrm{corr}}|\tau_\pm\sigma_\mu|\pi_1\nu_1\nu_{2\mathrm{corr}}\rangle = \delta(\nu_1',\nu_2)[\delta(\pi_1',\pi_1)\langle\pi'_{2\mathrm{corr}}|\tau_\pm\sigma_\mu|\nu_{1\mathrm{corr}}\rangle - \delta(\pi_2',\pi_1)\langle\pi'_{1\mathrm{corr}}|\tau_\pm\sigma_\mu|\nu_{1\mathrm{corr}}\rangle] - \delta(\nu_1',\nu_1)[\delta(\pi_1',\pi_1)\langle\pi'_{2\mathrm{corr}}|\tau_\pm\sigma_\mu|\nu_{2\mathrm{corr}}\rangle - \delta(\pi_2',\pi_1)\langle\pi'_{1\mathrm{corr}}|\tau_\pm\sigma_\mu|\nu_{2\mathrm{corr}}\rangle], \tag{28}$$

$$\langle\nu_1'\nu_2'\nu'_{3\mathrm{corr}}|\tau_\pm\sigma_{-\mu}|\pi_1\nu_1\nu_{2\mathrm{corr}}\rangle = \delta(\nu_2',\nu_1)\delta(\nu_3',\nu_2)\langle\nu'_{1\mathrm{corr}}|\tau_\pm\sigma_{-\mu}|\pi_{1\mathrm{corr}}\rangle - \delta(\nu_1',\nu_1)\delta(\nu_3',\nu_2)\langle\nu'_{2\mathrm{corr}}|\tau_\pm\sigma_{-\mu}|\pi_{1\mathrm{corr}}\rangle + \delta(\nu_1',\nu_1)\delta(\nu_2',\nu_2)\langle\nu'_{3\mathrm{corr}}|\tau_\pm\sigma_{-\mu}|\pi_{1\mathrm{corr}}\rangle, \tag{29}$$

and for the parent nuclei with an odd neutron

$$\langle\pi_1'\nu_1'\nu'_{2\mathrm{corr}}|\tau_\pm\sigma_\mu|\nu_1\nu_2\nu_{3\mathrm{corr}}\rangle = \delta(\nu_1',\nu_2)\delta(\nu_2',\nu_3)\langle\pi'_{1\mathrm{corr}}|\tau_\pm\sigma_\mu|\nu_{1\mathrm{corr}}\rangle - \delta(\nu_1',\nu_1)\delta(\nu_2',\nu_3)\langle\pi'_{1\mathrm{corr}}|\tau_\pm\sigma_\mu|\nu_{2\mathrm{corr}}\rangle + \delta(\nu_1',\nu_1)\delta(\nu_2',\nu_2)\langle\pi'_{1\mathrm{corr}}|\tau_\pm\sigma_\mu|\nu_{3\mathrm{corr}}\rangle, \tag{30}$$

$$\langle\pi_1'\nu_1'\nu'_{2\mathrm{corr}}|\tau_\pm\sigma_{-\mu}|\pi_1\pi_2\nu_{1\mathrm{corr}}\rangle = \delta(\pi_1',\pi_2)[\delta(\nu_1',\nu_1)\langle\nu'_{2\mathrm{corr}}|\tau_\pm\sigma_{-\mu}|\pi_{1\mathrm{corr}}\rangle - \delta(\nu_2',\nu_1)\langle\nu'_{1\mathrm{corr}}|\tau_\pm\sigma_{-\mu}|\pi_{1\mathrm{corr}}\rangle] - \delta(\pi_1',\pi_1)[\delta(\nu_1',\nu_1)\langle\nu'_{2\mathrm{corr}}|\tau_\pm\sigma_{-\mu}|\pi_{2\mathrm{corr}}\rangle - \delta(\nu_2',\nu_1)\langle\nu'_{1\mathrm{corr}}|\tau_\pm\sigma_{-\mu}|\pi_{2\mathrm{corr}}\rangle], \tag{31}$$

$$\langle\pi_1'\pi_2'\pi'_{3\mathrm{corr}}|\tau_\pm\sigma_\mu|\pi_1\pi_2\nu_{1\mathrm{corr}}\rangle = \delta(\pi_2',\pi_1)\delta(\pi_3',\pi_2)\langle\pi'_{1\mathrm{corr}}|\tau_\pm\sigma_\mu|\nu_{1\mathrm{corr}}\rangle - \delta(\pi_1',\pi_1)\delta(\pi_3',\pi_2)\langle\pi'_{2\mathrm{corr}}|\tau_\pm\sigma_\mu|\nu_{1\mathrm{corr}}\rangle + \delta(\pi_1',\pi_1)\delta(\pi_2',\pi_2)\langle\pi'_{3\mathrm{corr}}|\tau_\pm\sigma_\mu|\nu_{1\mathrm{corr}}\rangle. \tag{32}$$

Low-lying states in an odd-odd nucleus were expressed in the quasiparticle picture by proton-neutron pair states (two quasiparticle states) or by states that were obtained by adding two proton or two-neutron quasiparticles (four quasiparticle states). Transitions from the former states were described earlier. Phonon-correlated four quasiparticle states can be constructed similarly to the two and three quasiparticle states. Also, in this case, transition amplitudes for the four quasiparticle states were reduced into those for the correlated one quasiparticle states

$$<\pi_1'\pi_2'\nu_1'\nu'_{2\mathrm{corr}}|\tau_\pm\sigma_{-\mu}|\pi_1\pi_2\pi_3\nu_{1\mathrm{corr}}> = \delta(\nu_2',\nu_1)[\delta(\pi_1',\pi_2)\delta(\pi_2',\pi_3)<\nu'_{1\mathrm{corr}}|\tau_\pm\sigma_{-\mu}|\pi_{1\mathrm{corr}}> - \delta(\pi_1',\pi_1)\delta(\pi_2',\pi_3)<\nu'_{1\mathrm{corr}}|\tau_\pm\sigma_{-\mu}|\pi_{2\mathrm{corr}}> + \delta(\pi_1',\pi_1)\delta(\pi_2',\pi_2)<\nu'_{1\mathrm{corr}}|\tau_\pm\sigma_{-\mu}|\pi_{3\mathrm{corr}}>] - \delta(\nu_1',\nu_1)[\delta(\pi_1',\pi_2)\delta(\pi_2',\pi_3)<\nu'_{2\mathrm{corr}}|\tau_\pm\sigma_{-\mu}|\pi_{1\mathrm{corr}}> - \delta(\pi_1',\pi_1)\delta(\pi_2',\pi_3)<\nu'_{2\mathrm{corr}}|\tau_\pm\sigma_{-\mu}|\pi_{2\mathrm{corr}}> + \delta(\pi_1',\pi_1)\delta(\pi_2',\pi_2)<\nu'_{2\mathrm{corr}}|\tau_\pm\sigma_{-\mu}|\pi_{3\mathrm{corr}}>], \tag{33}$$

$$\begin{aligned}
&< \pi_1'\pi_2'\pi_3'\pi_{4\mathrm{corr}}'|\tau_\pm\sigma_\mu|\pi_1\pi_2\pi_3\nu_{1\mathrm{corr}} > \\
&= -\delta(\pi_2',\pi_1)\delta(\pi_3',\pi_2)\delta(\pi_4',\pi_3) < \pi_{1\mathrm{corr}}'|\tau_\pm\sigma_\mu|\nu_{1\mathrm{corr}} > \\
&+ \delta(\pi_1',\pi_1)\delta(\pi_3',\pi_2)\delta(\pi_4',\pi_3) < \pi_{2\mathrm{corr}}'|\tau_\pm\sigma_\mu|\nu_{1\mathrm{corr}} > \\
&- \delta(\pi_1',\pi_1)\delta(\pi_2',\pi_2)\delta(\pi_4',\pi_3) < \pi_{3\mathrm{corr}}'|\tau_\pm\sigma_\mu|\nu_{1\mathrm{corr}} > \\
&+ \delta(\pi_1',\pi_1)\delta(\pi_2',\pi_2)\delta(\pi_3',\pi_3) < \pi_{4\mathrm{corr}}'|\tau_\pm\sigma_\mu|\nu_{1\mathrm{corr}} >,
\end{aligned} \tag{34}$$

$$\begin{aligned}
&< \pi_1'\pi_2'\nu_1'\nu_{2\mathrm{corr}}'|\tau_\pm\sigma_\mu|\pi_1\nu_1\nu_2\nu_{3\mathrm{corr}} > \\
&= \delta(\pi_1',\pi_1)[\delta(\nu_1',\nu_2)\delta(\nu_2',\nu_3) < \pi_{2\mathrm{corr}}'|\tau_\pm\sigma_\mu|\nu_{1\mathrm{corr}} > \\
&- \delta(\nu_1',\nu_1)\delta(\nu_2',\nu_3) < \pi_{2\mathrm{corr}}'|\tau_\pm\sigma_\mu|\nu_{2\mathrm{corr}} > \\
&+ \delta(\nu_1',\nu_1)\delta(\nu_2',\nu_2) < \pi_{2\mathrm{corr}}'|\tau_\pm\sigma_\mu|\nu_{3\mathrm{corr}} >] \\
&- \delta(\pi_2',\pi_1)[\delta(\nu_1',\nu_2)\delta(\nu_2',\nu_3) < \pi_{1\mathrm{corr}}'|\tau_\pm\sigma_\mu|\nu_{1\mathrm{corr}} > \\
&- \delta(\nu_1',\nu_1)\delta(\nu_2',\nu_3) < \pi_{1\mathrm{corr}}'|\tau_\pm\sigma_\mu|\nu_{2\mathrm{corr}} > \\
&+ \delta(\nu_1',\nu_1)\delta(\nu_2',\nu_2) < \pi_{1\mathrm{corr}}'|\tau_\pm\sigma_\mu|\nu_{3\mathrm{corr}} >],
\end{aligned} \tag{35}$$

$$\begin{aligned}
&< \nu_1'\nu_2'\nu_3'\nu_{4\mathrm{corr}}'|\tau_\pm\sigma_{-\mu}|\pi_1\nu_1\nu_2\nu_{3\mathrm{corr}} > \\
&= +\delta(\nu_2',\nu_1)\delta(\nu_3',\nu_2)\delta(\nu_4',\nu_3) < \nu_{1\mathrm{corr}}'|\tau_\pm\sigma_{-\mu}|\pi_{1\mathrm{corr}} > \\
&- \delta(\nu_1',\nu_1)\delta(\nu_3',\nu_2)\delta(\nu_4',\nu_3) < \nu_{2\mathrm{corr}}'|\tau_\pm\sigma_{-\mu}|\pi_{1\mathrm{corr}} > \\
&+ \delta(\nu_1',\nu_1)\delta(\nu_2',\nu_2)\delta(\nu_4',\nu_3) < \nu_{3\mathrm{corr}}'|\tau_\pm\sigma_{-\mu}|\pi_{1\mathrm{corr}} > \\
&- \delta(\nu_1',\nu_1)\delta(\nu_2',\nu_2)\delta(\nu_3',\nu_3) < \nu_{4\mathrm{corr}}'|\tau_\pm\sigma_{-\mu}|\pi_{1\mathrm{corr}} > .
\end{aligned} \tag{36}$$

The antisymmetrization of the quasi-particles was duly considered for each of these amplitudes.

$\pi_4' > \pi_3' > \pi_2' > \pi_1'$, $\nu_4' > \nu_3' > \nu_2' > \nu_1'$, $\pi_4 > \pi_3 > \pi_2 > \pi_1$, $\nu_4 > \nu_3 > \nu_2 > \nu_1$.

The GT transitions were considered for each phonon's excited state. It was assumed that the quasiparticle in the parent nucleus occupies the same orbit as the excited phonons.

The form of the Hamiltonian for a many-particle QRPA system is

$$H_{\mathrm{QRPA}} = H_{\mathrm{sp}} + \hat{V}_{\mathrm{pairing}} + \hat{V}_{\mathrm{pp(GT)}} + \hat{V}_{\mathrm{ph(GT)}}, \tag{37}$$

where H_{sp} is the single-particle Hamiltonian whose energies and wave-vectors were calculated using the deformed Nilsson model [64]. $\hat{V}_{\mathrm{pp(GT)}}$ (Eq. (5)) and $\hat{V}_{\mathrm{ph(GT)}}$ (Eq. (7)) were introduced earlier in this section. The pairing correlations ($\hat{V}_{\mathrm{pairing}}$) were considered within the BCS formalism with fixed pairing gaps between proton-proton ($\Delta_{\pi\pi}$) and neutron-neutron ($\Delta_{\nu\nu}$) systems. The values of pairing gaps were calculated using empirical formulae [65] between neutron-neutron ($\Delta_{\nu\nu}$) and proton-proton ($\Delta_{\pi\pi}$) systems. The expressions for these gaps were given by

$$\begin{aligned}
\Delta_{\nu\nu} &= \frac{(-1)^{1-Z+A}[S_\nu(A-1,Z) - 2S_\nu(A,Z) + S_\nu(A+1,Z)]}{4}, \\
\Delta_{\pi\pi} &= \frac{(-1)^{1+Z}[S_\pi(A-1,Z-1) - 2S_\pi(A,Z) + S_\pi(A+1,Z+1)]}{4},
\end{aligned} \tag{38}$$

where the proton and neutron separation energies, S_π and S_ν, respectively, were taken from [66] for cases where the latest experimental data [67] were not available. The nuclear deformation values were taken from [68], and the mass excess values were adopted from [67], The Nilsson oscillatory constant was chosen as

$$\Omega = \frac{45}{A^{1/3}} - \frac{25}{A^{2/3}}, \tag{39}$$

with the same values for neutrons and protons, and the Nilsson potential parameters were used to compute the weak rates.

We calculated both U1F and allowed transitions in this work. The allowed transitions depend only on spin (σ_μ) and iso-spin ($\tau_\pm$) type operators, while forbidden transitions also contain rY_{lm} where Y_{lm} are the associated spherical harmonics.

The matrix elements of the U1F transitions in the pp and ph directions were given by

$$V^{pp}_{\pi\nu,\pi'\nu'} = -2\kappa_{U1F} f_{\pi\nu}(\mu) f_{\pi'\nu'}(\mu), \tag{40}$$

$$V^{\mathrm{ph}}_{\pi\nu,\pi'\nu'} = 2\chi_{\mathrm{U1F}} f_{\pi\nu}(\mu) f_{\pi'\nu'}(\mu), \tag{41}$$

where the ph and pp interaction constants are respectively referred to as χ_{U1F} and κ_{U1F}, and the single-particle amplitude ($f_{\pi\nu}(\mu)$) of the U1F transition is given by

$$f_{\pi\nu}(\mu) = \langle\pi|\tau_- r[\sigma Y_1]_{2\mu}|\nu\rangle, \tag{42}$$

where the parities of the neutron ($|\nu\rangle$) and proton ($|\pi\rangle$) states are opposite to each other [1], and μ takes the values $0, \pm1$, and ±2. The parametrization of the ph and pp strength interaction constants, for both the allowed and U1F transitions, were adopted from [1].

The partial decay rate (λ_{if}) for any transition between the parent (i) and the daughter (f) states was calculated using

$$\lambda_{if} = \left(\frac{m_e^5 c^4 g^2}{2\hbar^7\pi^3}\right)\Phi_{if}(E_{\mathrm{fermi}}, T, \rho) B_{if}, \tag{43}$$

depending on the g (weak coupling constant) involving both vector (g_V) and axial-vector (g_A) type constants, B_{if} (reduced transition probabilities) and Φ_{if} (phase-space integrals). For the continuum (allowed) EC, these integrals were computed using

$$\Phi_{ij}^{\mathrm{EC}} = \int_{w_l}^{\infty} w(w^2-1)^{1/2}(w_m+w)^2(G_-)F(+Z,w)\,\mathrm{d}w, \quad (44)$$

while the allowed BD was calculated as follows:

$$\Phi_{ij}^{\mathrm{BD}} = \int_{1}^{w_m} w(w^2-1)^{1/2}(w_m-w)^2(1-G_-)F(+Z,w)\,\mathrm{d}w, \quad (45)$$

For the U1F transition, the expression of phase-space integrals (Φ_{if}^{U1F}) is given below

$$\Phi_{ij}^{\mathrm{U1F}} = \int_{1}^{w_m} \{w(w^2-1)^{1/2}(w_m-w)^2(1-G_-)[F_1(Z,w)(w_m-w)^2+F_2(Z,w)(w^2-1)]\}\,\mathrm{d}w. \quad (46)$$

In Eqs. (44)−(46), we used natural units ($\hbar = m_e = c = 1$). w denotes the total electron energy, which includes the kinetic and rest mass energies, and w_l signifies the energy threshold for EC, while w_m represents the total BD energy. The symbol G_- denotes the Fermi Dirac distribution function for electrons. The Fermi functions (F, F_1, and F_2) used in this study were adopted from [69].

The reduced transition probability (B_{if}) is given as

$$B_{if} = \left(\frac{g_A}{g_V}\right)^2 B(\mathrm{GT}_\pm)_{if} + B(F_\pm)_{if}, \quad (47)$$

where $B(\mathrm{GT}_\pm)_{if}$ and $B(F_\pm)_{if}$ are the GT and Fermi transition probabilities, respectively. In Eq. (47), the value of $\frac{g_A}{g_V} = -1.2694$ (taken from [70]). The expressions for these probabilities are

$$B(F_\pm)_{if} = \frac{|\langle f\|\hat{O}\|i\rangle|^2}{2J_i+1}; \qquad \hat{O} = \sum_l \tau_\pm^l, \quad (48)$$

and

$$B(\mathrm{GT}_\pm)_{if} = \frac{|\langle f\|\hat{O}\|i\rangle|^2}{2J_i+1}; \qquad \hat{O} = \sum_l \tau_\pm^l \sigma^l, \quad (49)$$

where the symbols have their usual meanings. For the U1F transition, the reduced probability is

$$B(\mathrm{U1F})_{if} = \frac{1}{6}\eta^2 w^2 - \frac{1}{6}\eta^2 w_m w + \frac{1}{12}\eta^2(w_m^2-1), \quad (50)$$

where

$$\eta = 2g_A(2J_i+1)^{-1/2}\langle f\| \sum_l r_l [C_1^l \times \vec{\sigma}]^2 \tau_-^l \|i\rangle,$$
$$C_{kk'} = \left(\frac{4\pi}{2l+1}\right)^{1/2} \mathbf{Y}_{kk'}, \quad (51)$$

The partial rates were summed over all states in the parent and daughter nuclei to obtain the required convergence in the rates. The expression for the total rate is given by

$$\lambda = \sum_{if} P_i \lambda_{if}, \quad (52)$$

where the excited state occupation probability (P_i) of the parent nuclei is determined by applying the normal Boltzmann distribution.

In Eq. (52), total rates (λ) have been determined using the pn-QRPA formalism, where state-by-state transitions between excited and ground states of the parent and daughter nuclei were considered when calculating the strength functions in a totally microscopic fashion. The rates based on the BA hypothesis were estimated by replicating the strength functions for all parent excited states with ground level strengths [30]. Hereafter, microscopic (*Full*) pn-QRPA rates and those based on the BA hypothesis would be referred to as λ_F and λ_{BA}, respectively.

To compare the λ_F and λ_{BA} rates, we introduce two new parameters. These are the ratios and average deviations of the calculated rates. The algebraic expressions for the ratio (R_i) and the average deviation ($\bar{R}$) are

$$R_i = \begin{cases} \lambda_F/\lambda_{\mathrm{BA}} & \text{if } \lambda_F \geq \lambda_{\mathrm{BA}} \\ \lambda_{\mathrm{BA}}/\lambda_F & \text{if } \lambda_F < \lambda_{\mathrm{BA}}, \end{cases} \quad (53)$$

$$\bar{R} = \frac{\sum_{i=1}^k R_i}{k}, \quad (54)$$

where k denotes the total count of temperature-density points considered in the analysis.

III. RESULTS AND DISCUSSIONS

As stated earlier, this study aims to present a quantitative analysis of the reliability of BA rates, especially for U1F transitions. Our work builds on our previous research, which focused only on allowed transitions [47]. For the current study, we selected a specific region comprising 106 nuclei with A and Z ranging from (70 – 208) and (27 – 82), respectively. This region is particularly sensitive to the r-process. The selected nuclei have been reported in theoretical [2–4, 6, 12, 14–16, 32, 49–52, 55] and experimental [25–27, 29, 48] works. To check the reliability of the current model, we first present a comparison between the *pn*-QRPA calculated strength distributions for allowed GT transitions and measured data. For this purpose, we applied a smearing technique involving Lorentzian fitting to the theoretical strength distributions with an artificial width based on the calculated spectrum. This technique has been commonly used [21–23, 71] to compare the experimental (measured in MeV^{-1} units) and theoretical strength distributions. A decent comparison between theory and experiment can be seen from Figs. 1–2 in $(GT)_+$ and $(GT)_-$ directions, respectively. In both of these figures, the GT strengths [MeV^{-1}] are plotted as a function of excitation energies [MeV] of the corresponding daughter nuclei (along the abscissa). It is noted that

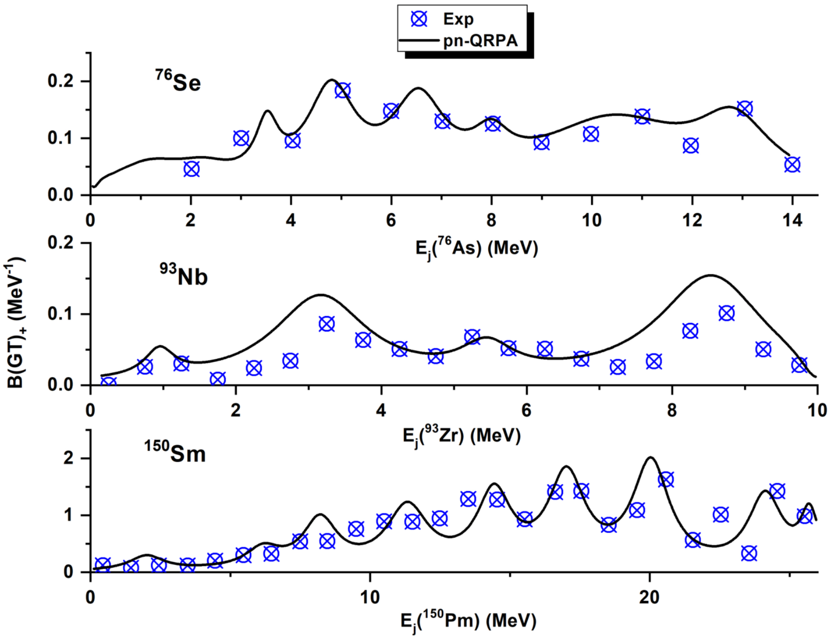

Fig. 1. (color online) Comparison of the *pn*-QRPA calculated GT_+ strength distributions of ^{76}Se, ^{93}Nb, and ^{150}Sm with measured data taken from [72], [71], and [22], respectively.

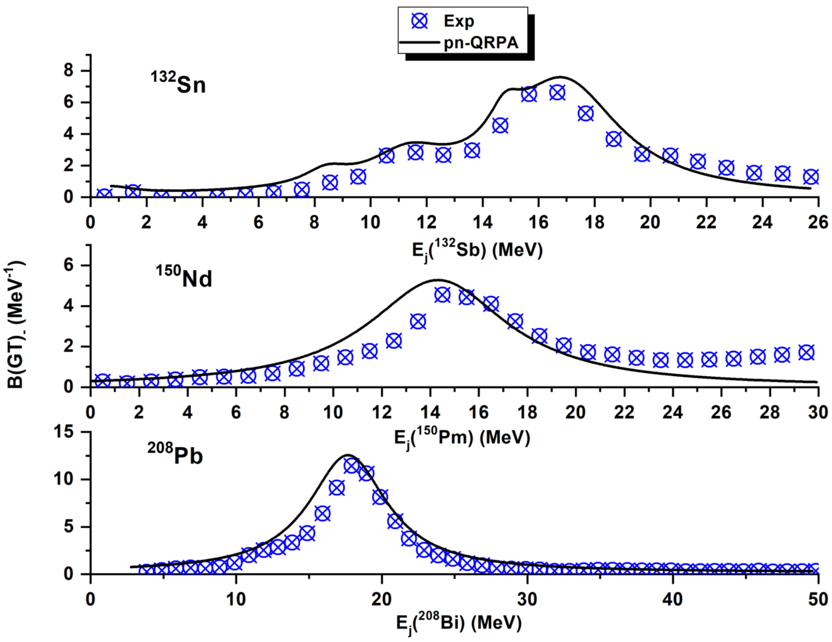

Fig. 2. (color online) Comparison of the *pn*-QRPA calculated GT_- strength distributions of ^{132}Sn, ^{150}Nd, and ^{208}Pb with measured data taken from the [21- 23], respectively.

the strength is well fragmented. After establishing the reliability of current model, we next proceed to further our investigation using the *pn*-QRPA model.

The current and Homma *et al.* [1] calculations used the same nuclear Hamiltonian in the framework of *pn*-QRPA with a schematic GT residual interaction. Additionally, incorporating the U1F transitions in our model was done per the recipe given in [1]. The reliability of the current model for calculating the U1F transitions was discussed earlier in [1]. Table 1 reproduces the data shown in [1] with the latest measured half-lives [67]. A decent agreement between the calculated and measured half-lives is obtained for ^{39}Ar and ^{41}Ca, for which β-decay is known experimentally to be dominated by U1F transitions. It may be seen from Table 1 that, for certain cases, taking only the allowed and U1F transitions into account overestimates the β-decay half-lives. This suggests that rank 0 and 1 FF transitions significantly contribute to these nuclei. Work on the code to include non-unique FF transitions in the stellar rate calculations is currently in progress, and we plan to report our findings in the near future.

As mentioned earlier, previous works focused only on the calculations and measurements of half-lives and beta-delayed neutron-emission probabilities for the nuclei currently under investigation. However, evaluating the reliability of the BA hypothesis in calculating the stellar rates for the selected pool of nuclei is of utmost importance. With this consideration, two sets of calculations (one each for the allowed and U1F rates) were performed separately for the EC and BD decays.

Table 1. Contribution of U1F transition to total β-decay for selected nuclei. $T^{All}_{1/2}$ is the partial half-life for the allowed β-decay. $T^{\rm total}_{1/2}$ is the total half-life, including both the allowed and U1F decays. Measured half-lives were taken from [67]. The dash indicates that the calculation predicts no allowed transition. The table was adopted from [1].

Nuclei	Decay mode	$\mathrm{T}^{\rm expt}_{1/2}$ /s	$\mathrm{T}^{\rm All}_{1/2}$ /s	$\mathrm{T}^{\rm total}_{1/2}$ /s	Contribution /%
^{36}P	β^-	$5.60\times10^{+00}$	$1.38\times10^{+02}$	$1.36\times10^{+02}$	1.7
^{37}S	β^-	$3.03\times10^{+02}$	$1.48\times10^{+02}$	$1.46\times10^{+02}$	1.6
^{38}Cl	β^-	$2.23\times10^{+03}$	–	$4.36\times10^{+08}$	100.0
^{39}Ar	β^-	$8.46\times10^{+09}$	–	$7.60\times10^{+09}$	100.0
^{41}Ca	β^+	$3.14\times10^{+12}$	–	$7.40\times10^{+11}$	100.0
^{133}Sn	β^-	$1.46\times10^{+00}$	$5.07\times10^{+01}$	$4.50\times10^{+01}$	11.4
^{134}Sb	β^-	7.80×10^{-01}	$3.71\times10^{+02}$	$3.40\times10^{+02}$	8.1
^{135}Te	β^-	$1.90\times10^{+01}$	$2.89\times10^{+03}$	$1.26\times10^{+03}$	56.3
^{136}I	β^-	$8.34\times10^{+01}$	$9.57\times10^{+03}$	$4.96\times10^{+03}$	48.2
^{137}Xe	β^-	$2.29\times10^{+02}$	$4.51\times10^{+03}$	$3.72\times10^{+03}$	17.4
^{138}Cs	β^-	$1.95\times10^{+03}$	$6.83\times10^{+04}$	$3.74\times10^{+04}$	45.2
^{139}Ba	β^-	$4.98\times10^{+03}$	$3.74\times10^{+04}$	$3.55\times10^{+04}$	5.0
^{140}La	β^-	$1.45\times10^{+05}$	$8.79\times10^{+04}$	$8.59\times10^{+04}$	2.3
^{141}Ce	β^-	$2.81\times10^{+06}$	–	$1.31\times10^{+09}$	100.0
^{142}Pr	β^-	$6.88\times10^{+04}$	–	$9.53\times10^{+11}$	100.0
^{144}Pm	β^+	$3.14\times10^{+07}$	–	$7.56\times10^{+10}$	100.0

In order to analyze the validity of the BA hypothesis for calculating the BD rates under stellar conditions, we chose three waiting point nuclei (^{82}Ge, ^{134}Te, and ^{201}Re). The selected nuclei have $N = 50$, $N = 82$ and $N = 126$, respectively. Accurate determination of the BD rates of these waiting point nuclei bears significance for the r-process nucleosynthesis. A comparison between the λ_F and $\lambda_{\rm BA}$ rates of the allowed and U1F transitions is presented in Figs. 3−5 in the BD direction. The effectiveness of applying the BA hypothesis for the EC nuclei is displayed in Figs. 6−8. Here, we selected ^{86}Kr, ^{150}Sm, and ^{207}Tl as study cases. The values of the rates are given in per-second units. For these figures, the three left panels (in the vertical direction) show both (*Full*) and BA U1F rates, whereas, the allowed rates are compared in the right panels. In these figures, $\lambda^{\rm BD}_{\rm All}$ and $\lambda^{\rm BD}_{\rm U1F}$ ($\lambda^{\rm EC}_{\rm All}$ and $\lambda^{\rm EC}_{\rm U1F}$) represent the allowed and U1F rates of the BD (EC) transitions, respectively. In this current study, we have calculated the rates for temperature range $T = (1 – 30)$ GK and density range ρY_e = (10^3 – 10^{11}) g/cm^3, roughly corresponding to the physical conditions pertinent to the r-process environment. Because of space consideration, the results have been reported at selected density snapshots: ρY_e = (10^4, 10^8, 10^{10} and 10^{11}) g/cm^3. Rates smaller than 10^{-15} s^{-1} are not shown in the figures.

A careful analysis of Figs. 3−5 shows that $\lambda_{\rm BA}$ of the U1F BD transitions are much bigger than λ_F. Table 2 shows the ratios (R_i) between BA and *Full* BD rates, calculated according to Eq. (53), for both the allowed GT and U1F transitions at predetermined physical conditions of the stellar core for three more nuclei. No entries are shown for ratios at core density ρY_e = 10^{11} g/cm^3 as the calculated rates are less than 10^{-100} s^{-1}. It is noted that, at times, the calculated rates are very small (λ < 10^{-5} s^{-1}). These very small numbers can change by orders of magnitude by a mere change of 0.5 MeV, or less, in parent or daughter excitation energies and are more reflective of the uncertainties in calculating the energies [7]. Consequently, we show two different average deviation values towards the end of Table 2. The first entry is the one defined by Eq. (54). The second entry (marked with an *) is the one excluding entries where the calculated rates are less than 10^{-5} s^{-1}. Table 3 depicts similar data for EC rates. Our results show that the U1F BD rates, calculated by incorporating the BA hypothesis, are largely overestimated relative to the microscopic (*Full*) rates by up to 4–5 orders of magnitude. On the other hand, Tables 2 – 3 show that for the EC (U1F and allowed) and allowed BD, the BA rates are, on average, lower than the *Full* rates.

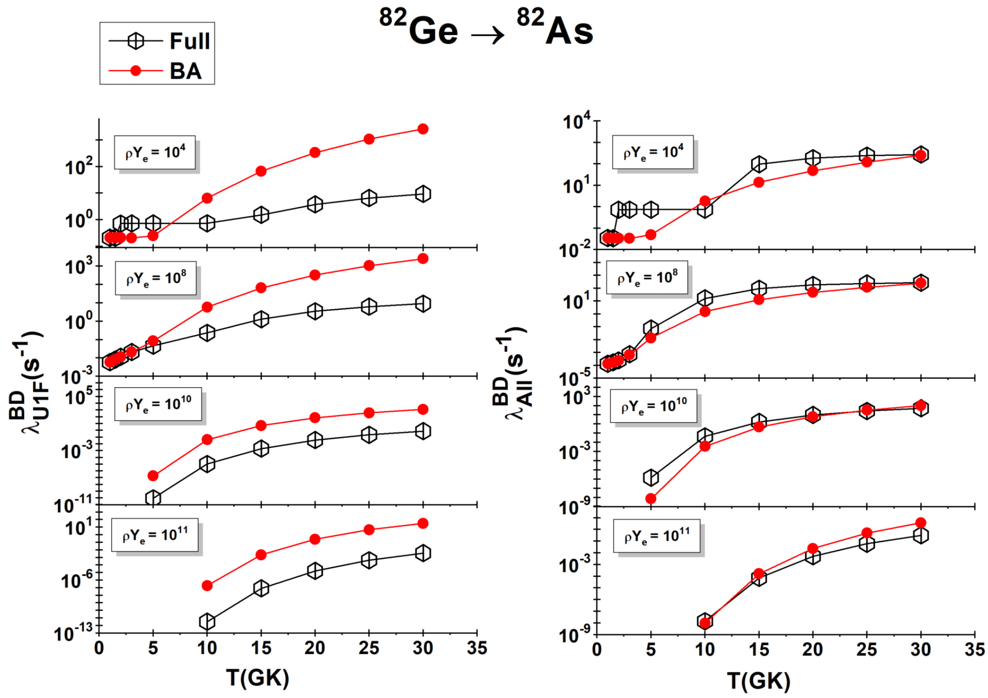

Fig. 3. (color online) Calculated *Full* (microscopic) and BA (based on BA hypothesis) BD rates [s^{-1}] for the U1F ($\lambda^{\rm BD}_{\rm U1F}$) and allowed ($\lambda^{\rm BD}_{All}$) transitions on ^{82}Ge at selected stellar densities (ρY_e [g/cm^3]) and temperatures.

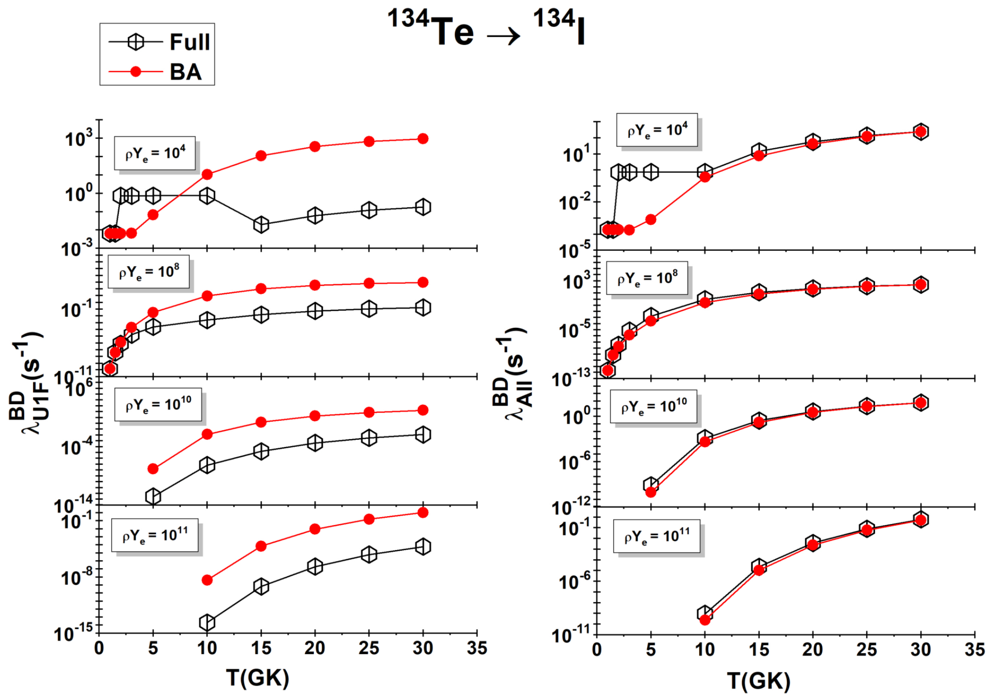

Fig. 4. (color online) Same as Fig. 3 but for ^{134}Te.

The total (allowed plus U1F) BA rates ($\lambda_{\rm BA}$[All + U1F]), in both EC and BD directions, deviate from total *Full* (λ_F[All + U1F]) rates, on average, by an order of magnitude or more. This difference can be seen from Table 4 and Table 5 for BD and EC, respectively. These tables show the total BA and *Full* rates and the ratios (R_i) between them.

There are three main causes of an increase in the calculated weak rate: (1) enlarged phase space; (2) bigger total GT strength distribution values; and (3) lower placement of the computed GT centroid. The calculated phase space and total GT strength distributions (along with

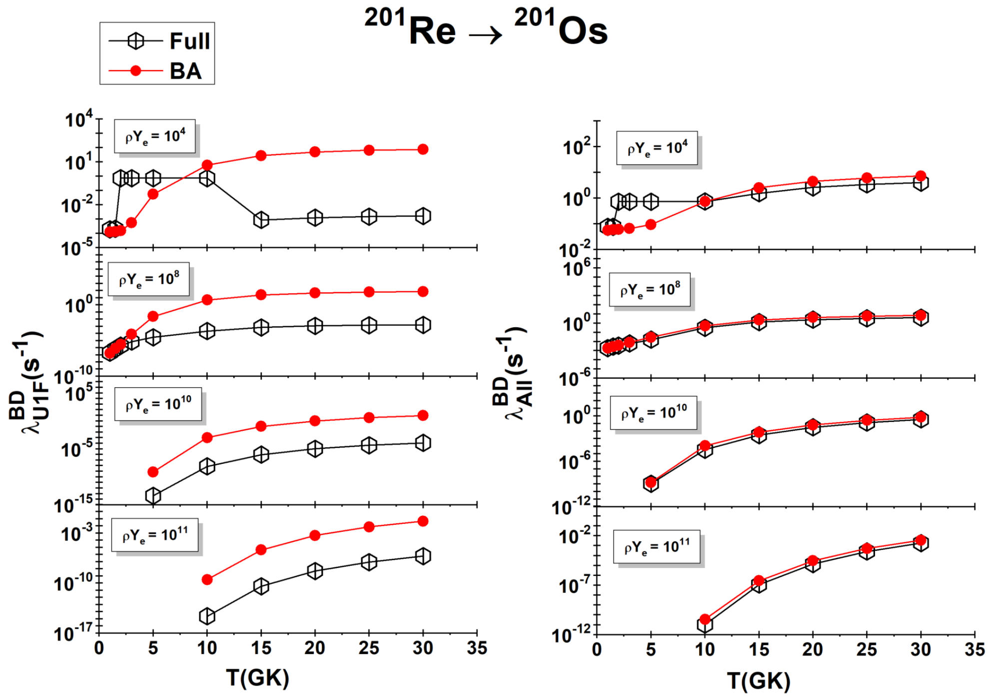

Fig. 5. (color online) Same as Fig. 3 but for ^{201}Re.

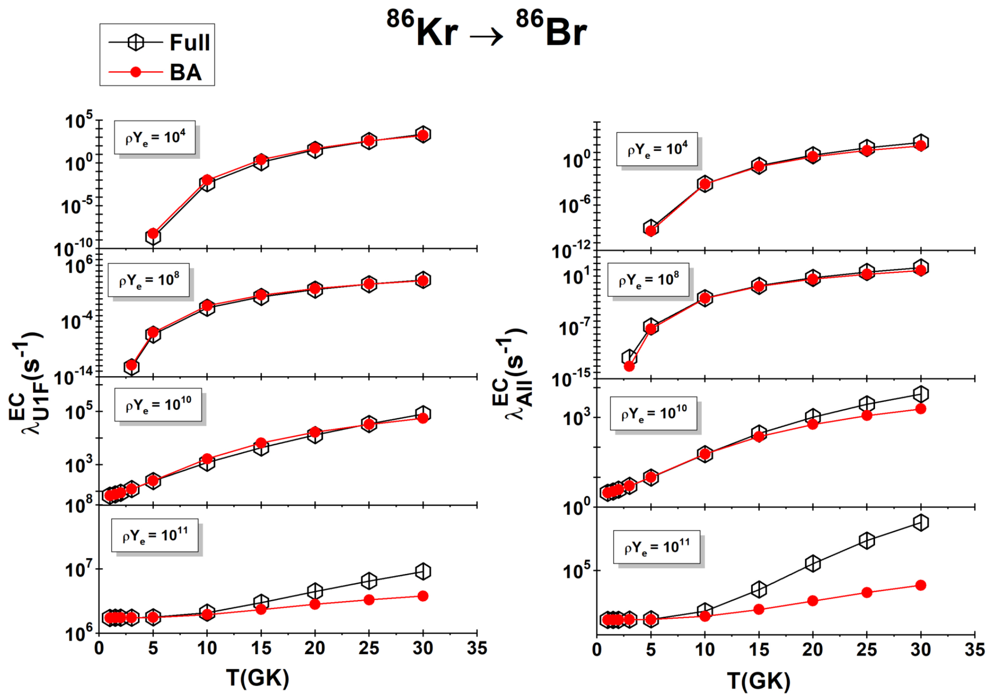

Fig. 6. (color online) Same as Fig. 3 but for the EC rates of the U1F ($\lambda^{\rm EC}_{\rm U1F}$) and allowed ($\lambda^{\rm EC}_{\rm All}$) transitions on ^{86}Kr.

centroid placement) are shown in Tables 6–8, respectively. The enhancement of $\lambda_{\rm BA}$ relative to the λ_F in U1F BD case is due to enlarged available phase spaces introduced by applying the BA hypothesis. Table 6 shows that the U1F computed phase spaces by invoking BA hypothesis are up to three orders of magnitude bigger for high core temperatures,. For low temperature and high density regions, the calculated BD rates approach zero because of choked phase spaces. In contrast, for the allowed GT rates in the BD direction, and for the U1F and allowed rates in the EC direction, the computed phase spaces (*Full* and BA) are comparable in magnitude (see Table 7 for three EC nuclei: ^{86}Kr, ^{150}Sm, and ^{207}Tl). Consequently, we note only a slight variation, typically of a few factors,

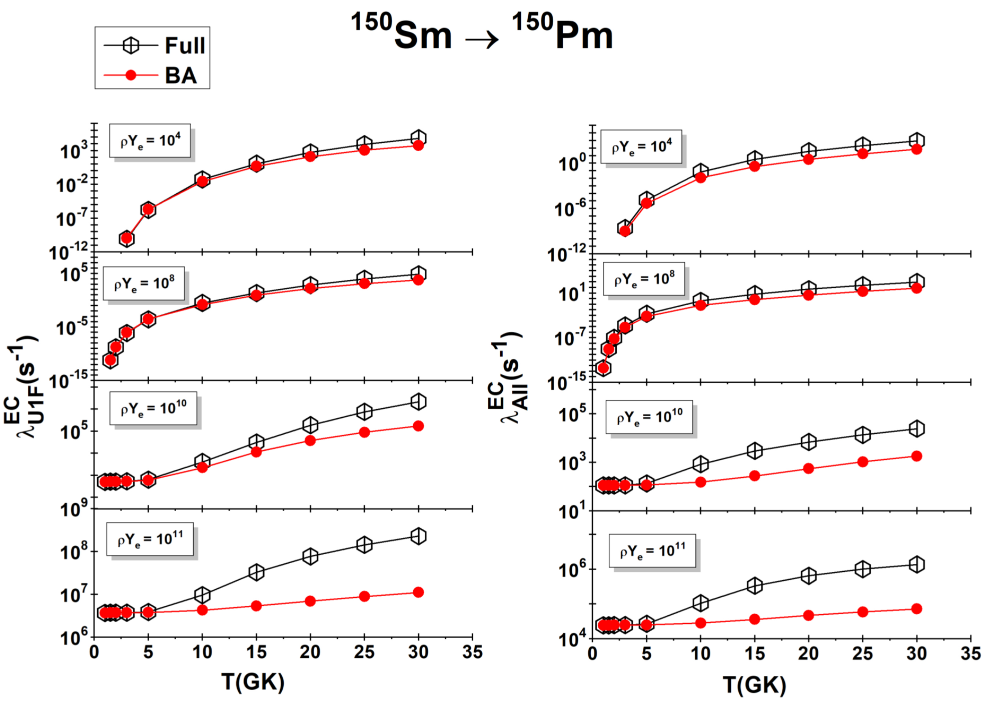

Fig. 7. (color online) Same as Fig. 6 but for the EC rates on ^{150}Sm.

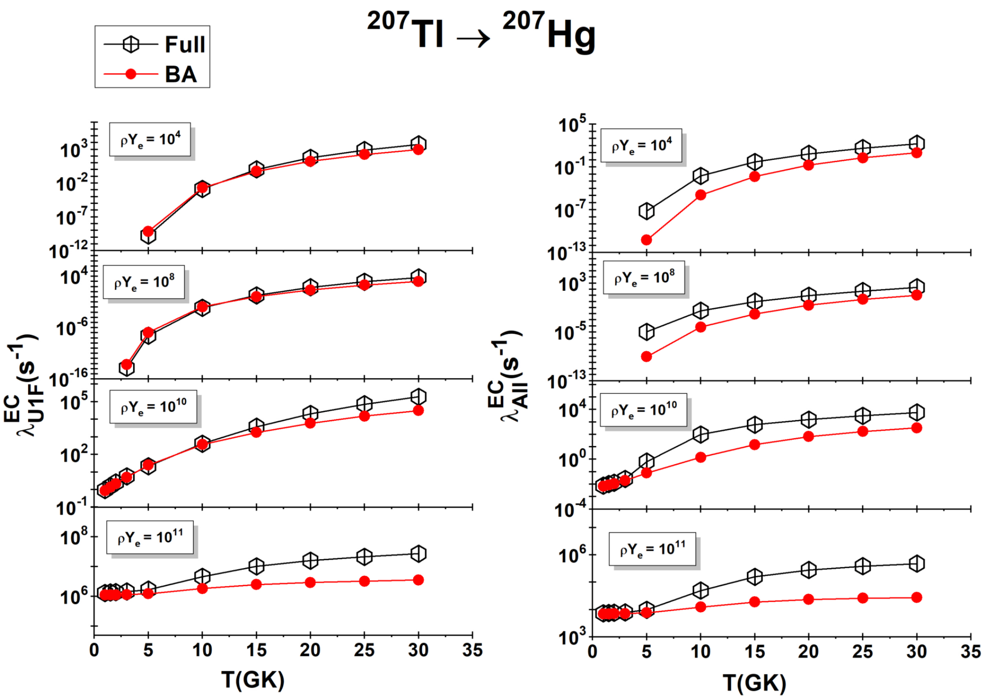

Fig. 8. (color online) Same as Fig. 6 but for EC rates on ^{207}Tl.

in the values of BA and *Full* rates other than U1F BD rates. Besides the available phase space values, another reason for the enhancement of the U1F BD $\lambda_{\rm BA}$ rates is the larger magnitude of the total GT strength. Table 8 shows the computed cumulative GT strength and placement of the GT centroid for the six selected nuclei. This table depicts the GT strength distribution data for the first 10 parent excited states. The cut-off energy in the daughter states is 15 MeV. Overall, larger dissimilarities in the available phase spaces between the microscopic and BA recipes for the U1F BD transitions and bigger values of total strength distributions result in a much larger devi-

Table 2. Comparison of the BA ($\lambda_{\rm BA}$) and *Full* (λ_F) β-decay rates for three selected nuclei as a function of core temperature (T (GK)) and density (ρY_e (g/cm^3)). The ratios (R_i) and average deviation ($\bar{R}$) are defined in Eq. (53) and Eq. (54), respectively. The computed R_i values, where λ_F and/or $\lambda_{\rm BA}$ rates are less than 10^{-5} s^{-1}, are marked with *. $\bar{R}^{(*)}$ are the computed average deviations excluding ratios marked with *.

T	ρ**Y**$_e$	^{82}Ge				^{134}Te				^{201}Re			
		R_i [All]		R_i [U1F]		R_i [All]		R_i [U1F]		R_i [All]		R_i [U1F]	
		$\lambda_F \geq \lambda_{\rm BA}$	$\lambda_{\rm BA} > \lambda_F$	$\lambda_F \geq \lambda_{\rm BA}$	$\lambda_{\rm BA} > \lambda_F$	$\lambda_F \geq \lambda_{\rm BA}$	$\lambda_{\rm BA} > \lambda_F$	$\lambda_F \geq \lambda_{\rm BA}$	$\lambda_{\rm BA} > \lambda_F$	$\lambda_F \geq \lambda_{\rm BA}$	$\lambda_{\rm BA} > \lambda_F$	$\lambda_F \geq \lambda_{\rm BA}$	$\lambda_{\rm BA} > \lambda_F$
1	10^4	1.0			1.0	1.0			1.0	1.3		1.5	
5	10^4	2.5			1.2	3.7			12.2		1.2		264.9
10	10^4	9.9			17.3	3.3			1840.8		1.5		15452.5
20	10^4	3.8			86.7	1.4			5821.0		1.7		39355.0
30	10^4	1.1			272.3	1.0			5164.2		1.8		46025.7
1	10^8	1.0			1.0	1.0$^{(*)}$			1.0$^{(*)}$	1.1		1.1	
5	10^8	5.3			1.8	6.5			139.0		1.8		824.1
10	10^8	10.7			25.2	3.6			3698.3		1.6		22335.7
20	10^8	3.8			93.1	1.4			6295.1		1.7		41115.0
30	10^8	1.1			279.3	1.0			5284.5		1.8		46558.6
1	10^{11}	—	—	—	—	—	—	—	—	—	—	—	—
5	10^{11}	24.1$^{(*)}$			40457.6$^{(*)}$	6.1$^{(*)}$			53210.8$^{(*)}$		1.5$^{(*)}$		17418.1$^{(*)}$
10	10^{11}	1.4$^{(*)}$			58210.3$^{(*)}$	3.8$^{(*)}$			199067.3$^{(*)}$		3.4$^{(*)}$		133967.7$^{(*)}$
20	10^{11}		4.7		15417.0	1.6			45081.7$^{(*)}$		2.1		97949.0$^{(*)}$
30	10^{11}		12.0		8609.9	1.2			17458.2		2.0		78343.0$^{(*)}$
$\bar{\mathbf{R}}$		5.9		8819.6		2.6		24505.4		1.7		38543.7	
$\bar{\mathbf{R}}^{(*)}$		4.7		2067.2		2.3		4571.4		1.6		23548.1	

Table 3. Same as Table 2 but for three r-process EC nuclei.

T	ρ**Y**$_e$	^{86}Kr				^{150}Sm				^{207}Tl			
		R_i [All]		R_i [U1F]		R_i [All]		R_i [U1F]		R_i [All]		R_i [U1F]	
		$\lambda_F \geq \lambda_{\rm BA}$	$\lambda_{\rm BA} > \lambda_F$	$\lambda_F \geq \lambda_{\rm BA}$	$\lambda_{\rm BA} > \lambda_F$	$\lambda_F \geq \lambda_{\rm BA}$	$\lambda_{\rm BA} > \lambda_F$	$\lambda_F \geq \lambda_{\rm BA}$	$\lambda_{\rm BA} > \lambda_F$	$\lambda_F \geq \lambda_{\rm BA}$	$\lambda_{\rm BA} > \lambda_F$	$\lambda_F \geq \lambda_{\rm BA}$	$\lambda_{\rm BA} > \lambda_F$
1	10^4	1.2×10$^{+08(*)}$			2.1$^{(*)}$	3.2$^{(*)}$			1.2$^{(*)}$	5.0×10$^{+21(*)}$			6.0$^{(*)}$
5	10^4	2.5$^{(*)}$			2.4$^{(*)}$	2.9$^{(*)}$			1.2$^{(*)}$	1.2×10$^{+04(*)}$			4.1$^{(*)}$
10	10^4	1.1			2.4	5.9		2.0		485.3			1.5
20	10^4	1.6			1.5	11.6		4.3		37.5		3.2	
30	10^4	2.8		1.3		12.7		11.5		19.3		6.0	
1	10^8	5.1×10$^{+07(*)}$			2.1 $^{(*)}$	1.0 $^{(*)}$			1.1$^{(*)}$	4.7×10$^{+21(*)}$			6.0$^{(*)}$
5	10^8	2.4$^{(*)}$			2.4$^{(*)}$	2.9			1.2	1.2×10$^{+04(*)}$			4.1$^{(*)}$
10	10^8	1.1			2.4	6.0		2.0		479.7			1.5
20	10^8	1.6			1.5	11.6		4.3		37.4		3.2	
30	10^8	2.8		1.3		12.7		11.5		19.3		6.0	
1	10^{11}	1.0		1.0		1.0		1.0		1.1		1.2	
5	10^{11}	1.0		1.0		1.1		1.0		1.3		1.4	
10	10^{11}	1.1		1.1		3.7		2.2		4.0		2.5	
20	10^{11}	2.6		1.6		13.9		11.1		12.0		5.4	
30	10^{11}	4.8		2.4		18.9		20.7		17.5		7.6	
$\bar{\mathbf{R}}$		1.1×10^{+07}		1.8		7.3		5.1		6.4×10^{+20}		4.0	
$\bar{\mathbf{R}}^{(*)}$		2.0		1.6		8.5		6.1		101.3		3.6	

Table 4. Comparison of the total BA (λ_{BA}[All+U1F]) and *Full* (λ_F[All+U1F]) β-decay rates for three selected nuclei as a function of core temperature (T (GK)) and density (ρY_e (g/cm^3)). The ratios (R_i) and average deviation ($\bar{R}$) are defined in Eq. (53) and Eq. (54), respectively. The computed R_i values, where $\lambda_F > \lambda_{BA}$, are marked with *.

T	ρY_e	^{82}Ge			^{134}Te			^{201}Re		
		λ_F[All+U1F]	λ_{BA}[All+U1F]	R_i ($\lambda_{BA} \geq \lambda_F$)	λ_F[All+U1F]	λ_{BA}[All+U1F]	R_i ($\lambda_{BA} \geq \lambda_F$)	λ_F[All+U1F]	λ_{BA}[All+U1F]	R_i ($\lambda_{BA} \geq \lambda_F$)
1	10^4	2.47×10^{-01}	2.47×10^{-01}	1.0	6.66×10^{-03}	6.66×10^{-03}	1.0	7.61×10^{-02}	5.71×10^{-02}	1.3(*)
5	10^4	3.29×10^{-01}	3.02×10^{-01}	1.1(*)	8.51×10^{-03}	6.80×10^{-02}	8.0	7.75×10^{-02}	1.49×10^{-01}	1.9
10	10^4	$1.85\times10^{+01}$	$8.33\times10^{+00}$	2.2(*)	$1.18\times10^{+00}$	$1.10\times10^{+01}$	9.3	5.05×10^{-01}	$6.78\times10^{+00}$	13.4
20	10^4	$1.89\times10^{+02}$	$3.79\times10^{+02}$	2.0	$5.76\times10^{+01}$	$3.98\times10^{+02}$	6.9	$2.62\times10^{+00}$	$5.45\times10^{+01}$	20.8
30	10^4	$2.82\times10^{+02}$	$2.80\times10^{+03}$	10.0	$2.47\times10^{+02}$	$1.18\times10^{+03}$	4.8	$4.06\times10^{+00}$	$8.31\times10^{+01}$	20.5
1	10^8	6.02×10^{-03}	6.02×10^{-03}	1.0	1.48×10^{-10}	1.48×10^{-10}	1.0	1.96×10^{-03}	1.83×10^{-03}	1.1(*)
5	10^8	1.19×10^{-01}	9.85×10^{-02}	1.2(*)	1.94×10^{-03}	3.44×10^{-02}	17.8	1.57×10^{-02}	5.31×10^{-02}	3.4
10	10^8	$1.65\times10^{+01}$	$7.41\times10^{+00}$	2.2(*)	$1.00\times10^{+00}$	$9.63\times10^{+00}$	9.6	3.18×10^{-01}	$5.27\times10^{+00}$	16.6
20	10^8	$1.83\times10^{+02}$	$3.73\times10^{+02}$	2.0	$5.58\times10^{+01}$	$3.87\times10^{+02}$	6.9	$2.42\times10^{+00}$	$5.17\times10^{+01}$	21.3
30	10^8	$2.78\times10^{+02}$	$2.79\times10^{+03}$	10.1	$2.44\times10^{+02}$	$1.17\times10^{+03}$	4.8	$3.95\times10^{+00}$	$8.14\times10^{+01}$	20.6
1	10^{11}	—	—	—	—	—	—	—	—	—
5	10^{11}	1.81×10^{-19}	4.15×10^{-19}	2.3	1.98×10^{-22}	1.79×10^{-21}	9.1	1.26×10^{-22}	2.70×10^{-22}	2.1
10	10^{11}	1.44×10^{-08}	2.00×10^{-07}	13.9	8.95×10^{-10}	4.37×10^{-09}	4.9	1.05×10^{-11}	3.39×10^{-10}	32.2
20	10^{11}	5.05×10^{-03}	2.83×10^{-01}	55.9	3.78×10^{-03}	1.14×10^{-02}	3.0	1.41×10^{-05}	4.97×10^{-04}	35.2
30	10^{11}	3.19×10^{-01}	$3.58\times10^{+01}$	112.1	6.01×10^{-01}	$1.57\times10^{+00}$	2.6	1.79×10^{-03}	5.04×10^{-02}	28.1
	$\bar{R}$			15.5			6.4			15.6

Table 5. Same as Table 4 but for the three *r*-process EC nuclei. The computed R_i values, where $\lambda_{BA} > \lambda_F$, are marked with *.

T	ρY_e	^{86}Kr			^{150}Sm			^{207}Tl		
		λ_F[All+U1F]	λ_{BA}[All+U1F]	R_i ($\lambda_F \geq \lambda_{BA}$)	λ_F[All+U1F]	λ_{BA}[All+U1F]	R_i ($\lambda_F \geq \lambda_{BA}$)	λ_F[All+U1F]	λ_{BA}[All+U1F]	R_i ($\lambda_F \geq \lambda_{BA}$)
1	10^4	—	—	—	—	—	—	—	—	—
5	10^4	3.49×10^{-09}	6.33×10^{-09}	1.8(*)	1.63×10^{-05}	7.13×10^{-06}	2.3	6.81×10^{-08}	7.30×10^{-10}	93.3
10	10^4	5.10×10^{-03}	1.11×10^{-02}	2.2(*)	1.27×10^{-01}	3.96×10^{-02}	3.2	7.00×10^{-03}	2.06×10^{-03}	3.4
20	10^4	$4.04\times10^{+01}$	$5.60\times10^{+01}$	1.4(*)	$5.75\times10^{+02}$	$1.28\times10^{+02}$	4.5	$6.16\times10^{+01}$	$1.70\times10^{+01}$	3.6
30	10^4	$2.55\times10^{+03}$	$1.81\times10^{+03}$	1.4	$6.53\times10^{+04}$	$5.67\times10^{+03}$	11.5	$5.72\times10^{+03}$	$9.30\times10^{+02}$	6.2
1	10^8	—	—	—	—	—	—	—	—	—
5	10^8	5.50×10^{-07}	1.02×10^{-06}	1.9(*)	2.28×10^{-03}	1.03×10^{-03}	2.2	1.07×10^{-05}	1.18×10^{-07}	90.9
10	10^8	2.88×10^{-02}	6.28×10^{-02}	2.2(*)	7.09×10^{-01}	2.20×10^{-01}	3.2	3.92×10^{-02}	1.16×10^{-02}	3.4
20	10^8	$5.31\times10^{+01}$	$7.34\times10^{+01}$	1.4(*)	$7.56\times10^{+02}$	$1.68\times10^{+02}$	4.5	$8.10\times10^{+01}$	$2.24\times10^{+01}$	3.6
30	10^8	$2.77\times10^{+03}$	$1.96\times10^{+03}$	1.4	$7.08\times10^{+04}$	$6.14\times10^{+03}$	11.5	$6.20\times10^{+03}$	$1.01\times10^{+03}$	6.2
1	10^{11}	$1.77\times10^{+06}$	$1.77\times10^{+06}$	1.0	$3.72\times10^{+06}$	$3.72\times10^{+06}$	1.0	$1.32\times10^{+06}$	$1.13\times10^{+06}$	1.2
5	10^{11}	$1.80\times10^{+06}$	$1.80\times10^{+06}$	1.0	$3.92\times10^{+06}$	$3.81\times10^{+06}$	1.0	$1.70\times10^{+06}$	$1.24\times10^{+06}$	1.4
10	10^{11}	$2.14\times10^{+06}$	$1.99\times10^{+06}$	1.1	$9.70\times10^{+06}$	$4.29\times10^{+06}$	2.3	$4.61\times10^{+06}$	$1.84\times10^{+06}$	2.5
20	10^{11}	$4.61\times10^{+06}$	$2.88\times10^{+06}$	1.6	$7.77\times10^{+07}$	$6.98\times10^{+06}$	11.1	$1.61\times10^{+07}$	$2.94\times10^{+06}$	5.5
30	10^{11}	$9.50\times10^{+06}$	$3.87\times10^{+06}$	2.5	$2.31\times10^{+08}$	$1.12\times10^{+07}$	20.7	$2.77\times10^{+07}$	$3.60\times10^{+06}$	7.7
	$\bar{R}$			1.6			6.1			17.6

Table 6. Computed phase spaces of *Full* (microscopic) and BA rates for the allowed and U1F transitions at selected densities (ρY_e (g/cm^3)) and temperatures (T (GK)) in a stellar environment for three r-process BD nuclei.

T	ρY_e	^{82}Ge		^{134}Te		^{201}Re	
		Full	BA	Full	BA	Full	BA
				U1F			
1	10^4	$4.30\times10^{+09}$	$9.60\times10^{+09}$	$1.80\times10^{+09}$	$2.00\times10^{+09}$	$1.40\times10^{+11}$	$3.40\times10^{+11}$
5	10^4	$1.90\times10^{+10}$	$1.20\times10^{+11}$	$7.60\times10^{+09}$	$1.60\times10^{+10}$	$1.40\times10^{+11}$	$3.40\times10^{+11}$
10	10^4	$1.90\times10^{+10}$	$1.20\times10^{+11}$	$7.50\times10^{+09}$	$1.60\times10^{+10}$	$1.40\times10^{+11}$	$3.40\times10^{+11}$
20	10^4	$1.80\times10^{+10}$	$1.20\times10^{+11}$	$7.30\times10^{+09}$	$1.60\times10^{+10}$	$1.30\times10^{+11}$	$3.30\times10^{+11}$
30	10^4	$1.80\times10^{+10}$	$1.20\times10^{+11}$	$7.00\times10^{+09}$	$1.50\times10^{+10}$	$1.30\times10^{+11}$	$3.10\times10^{+11}$
1	10^8	$4.10\times10^{+09}$	$9.40\times10^{+09}$	$1.70\times10^{+09}$	$1.90\times10^{+09}$	$1.40\times10^{+11}$	$3.30\times10^{+11}$
5	10^8	$1.80\times10^{+10}$	$1.20\times10^{+11}$	$7.30\times10^{+09}$	$1.60\times10^{+10}$	$1.40\times10^{+11}$	$3.30\times10^{+11}$
10	10^8	$1.80\times10^{+10}$	$1.20\times10^{+11}$	$7.40\times10^{+09}$	$1.60\times10^{+10}$	$1.40\times10^{+11}$	$3.30\times10^{+11}$
20	10^8	$1.80\times10^{+10}$	$1.20\times10^{+11}$	$7.20\times10^{+09}$	$1.60\times10^{+10}$	$1.30\times10^{+11}$	$3.20\times10^{+11}$
30	10^8	$1.70\times10^{+10}$	$1.20\times10^{+11}$	$7.00\times10^{+09}$	$1.50\times10^{+10}$	$1.30\times10^{+11}$	$3.10\times10^{+11}$
1	10^{11}	$6.60\times10^{+04}$	$3.60\times10^{+06}$	1.60×10^{-13}	4.10×10^{-12}	1.70×10^{-37}	2.80×10^{-42}
5	10^{11}	$3.80\times10^{+07}$	$9.10\times10^{+09}$	$6.80\times10^{+04}$	$3.30\times10^{+07}$	1.90×10^{-01}	8.10×10^{-02}
10	10^{11}	$6.30\times10^{+07}$	$9.70\times10^{+09}$	$1.20\times10^{+06}$	$5.20\times10^{+07}$	$3.50\times10^{+04}$	$4.70\times10^{+04}$
20	10^{11}	$1.90\times10^{+08}$	$1.20\times10^{+10}$	$1.90\times10^{+07}$	$1.60\times10^{+08}$	$4.00\times10^{+07}$	$8.20\times10^{+07}$
30	10^{11}	$4.90\times10^{+08}$	$1.60\times10^{+10}$	$9.00\times10^{+07}$	$4.20\times10^{+08}$	$5.90\times10^{+08}$	$1.30\times10^{+09}$
				Allowed			
1	10^4	$1.80\times10^{+11}$	$2.70\times10^{+11}$	$2.80\times10^{+10}$	$3.00\times10^{+10}$	$9.60\times10^{+07}$	$7.30\times10^{+07}$
5	10^4	$1.10\times10^{+13}$	$1.10\times10^{+13}$	$6.90\times10^{+11}$	$6.90\times10^{+11}$	$9.50\times10^{+07}$	$7.20\times10^{+07}$
10	10^4	$1.10\times10^{+13}$	$1.10\times10^{+13}$	$6.90\times10^{+11}$	$6.90\times10^{+11}$	$9.10\times10^{+07}$	$6.90\times10^{+07}$
20	10^4	$1.10\times10^{+13}$	$1.10\times10^{+13}$	$6.90\times10^{+11}$	$6.90\times10^{+11}$	$8.20\times10^{+07}$	$6.20\times10^{+07}$
30	10^4	$1.10\times10^{+13}$	$1.10\times10^{+13}$	$6.80\times10^{+11}$	$6.80\times10^{+11}$	$7.40\times10^{+07}$	$5.70\times10^{+07}$
1	10^8	$1.80\times10^{+11}$	$2.70\times10^{+11}$	$2.80\times10^{+10}$	$3.00\times10^{+10}$	$6.70\times10^{+07}$	$5.10\times10^{+07}$
5	10^8	$1.10\times10^{+13}$	$1.10\times10^{+13}$	$6.90\times10^{+11}$	$6.90\times10^{+11}$	$7.10\times10^{+07}$	$5.40\times10^{+07}$
10	10^8	$1.10\times10^{+13}$	$1.10\times10^{+13}$	$6.90\times10^{+11}$	$6.90\times10^{+11}$	$7.80\times10^{+07}$	$5.90\times10^{+07}$
20	10^8	$1.10\times10^{+13}$	$1.10\times10^{+13}$	$6.80\times10^{+11}$	$6.90\times10^{+11}$	$7.80\times10^{+07}$	$6.00\times10^{+07}$
30	10^8	$1.10\times10^{+13}$	$1.10\times10^{+13}$	$6.80\times10^{+11}$	$6.80\times10^{+11}$	$7.30\times10^{+07}$	$5.60\times10^{+07}$
1	10^{11}	$1.00\times10^{+10}$	$1.00\times10^{+10}$	$6.50\times10^{+06}$	$6.50\times10^{+06}$	3.30×10^{-68}	5.60×10^{-70}
5	10^{11}	$4.50\times10^{+12}$	$4.50\times10^{+12}$	$1.40\times10^{+11}$	$1.40\times10^{+11}$	2.60×10^{-10}	1.20×10^{-10}
10	10^{11}	$4.60\times10^{+12}$	$4.60\times10^{+12}$	$1.50\times10^{+11}$	$1.50\times10^{+11}$	3.90×10^{-02}	2.60×10^{-02}
20	10^{11}	$4.80\times10^{+12}$	$4.80\times10^{+12}$	$1.60\times10^{+11}$	$1.60\times10^{+11}$	$1.40\times10^{+03}$	$1.00\times10^{+03}$
30	10^{11}	$5.00\times10^{+12}$	$5.00\times10^{+12}$	$1.80\times10^{+11}$	$1.80\times10^{+11}$	$6.20\times10^{+04}$	$4.60\times10^{+04}$

ation of $\lambda_{\rm BA}$ from λ_F. This later translated to larger magnitudes of R_i and $\bar{R}$ values. In the Appendix (Tables A1−A6), we show ratios and average ratios of nine new BD and EC nuclei, separately, for the allowed GT and U1F transitions.

For the BD rates (U1F and allowed) of N = 50 and N = 82 nuclei (Table 2), the calculated value of $R_{\rm i}$ equals 1.00 at T = 1 GK. This implies that at this temperature, both λ_F and $\lambda_{\rm BA}$ are identical. This core temperature corresponds roughly to the neon burning phases of the star. Consequently, we conclude that the BA hypothesis may be safely applied to stellar BD rates until the neon burning phases of massive stars. For heavy nuclei (*e.g.*, ^{201}Re), the BA fails even at T = 1 GK. Table 3 computes much smaller values of $\bar{R}$ for the EC rates. This means that the EC rates are less affected by the usage of the BA hypo-

Table 7. Same as Table 6 but for the three *r*-process EC nuclei.

T	ρY_e	^{86}Kr		^{150}Sm		^{207}Tl	
		Full	BA	Full	BA	Full	BA
		U1F					
1	10^4	$4.60\times10^{+10}$	$4.60\times10^{+10}$	$5.30\times10^{+01}$	$1.70\times10^{+10}$	$2.80\times10^{+10}$	$2.80\times10^{+10}$
5	10^4	$1.70\times10^{+12}$	$1.70\times10^{+12}$	$3.60\times10^{+12}$	$3.80\times10^{+12}$	$2.80\times10^{+10}$	$2.80\times10^{+10}$
10	10^4	$1.70\times10^{+12}$	$1.70\times10^{+12}$	$3.60\times10^{+12}$	$3.80\times10^{+12}$	$2.80\times10^{+10}$	$2.80\times10^{+10}$
20	10^4	$1.70\times10^{+12}$	$1.70\times10^{+12}$	$3.60\times10^{+12}$	$3.80\times10^{+12}$	$2.60\times10^{+10}$	$2.60\times10^{+10}$
30	10^4	$1.70\times10^{+12}$	$1.70\times10^{+12}$	$3.60\times10^{+12}$	$3.80\times10^{+12}$	$2.50\times10^{+10}$	$2.50\times10^{+10}$
1	10^8	$4.60\times10^{+10}$	$4.60\times10^{+10}$	1.80×10^{-07}	$1.60\times10^{+10}$	$2.70\times10^{+10}$	$2.70\times10^{+10}$
5	10^8	$1.70\times10^{+12}$	$1.70\times10^{+12}$	$3.60\times10^{+12}$	$3.80\times10^{+12}$	$2.70\times10^{+10}$	$2.70\times10^{+10}$
10	10^8	$1.70\times10^{+12}$	$1.70\times10^{+12}$	$3.60\times10^{+12}$	$3.80\times10^{+12}$	$2.70\times10^{+10}$	$2.70\times10^{+10}$
20	10^8	$1.70\times10^{+12}$	$1.70\times10^{+12}$	$3.60\times10^{+12}$	$3.80\times10^{+12}$	$2.60\times10^{+10}$	$2.60\times10^{+10}$
30	10^8	$1.70\times10^{+12}$	$1.70\times10^{+12}$	$3.60\times10^{+12}$	$3.80\times10^{+12}$	$2.40\times10^{+10}$	$2.40\times10^{+10}$
1	10^{11}	$1.10\times10^{+02}$	$1.10\times10^{+02}$	8.20×10^{-16}	3.80×10^{-13}	2.60×10^{-56}	2.60×10^{-56}
5	10^{11}	$5.90\times10^{+11}$	$5.90\times10^{+11}$	$9.60\times10^{+11}$	$9.60\times10^{+11}$	2.10×10^{-05}	2.10×10^{-05}
10	10^{11}	$5.90\times10^{+11}$	$5.90\times10^{+11}$	$9.80\times10^{+11}$	$9.80\times10^{+11}$	$2.40\times10^{+02}$	$2.40\times10^{+02}$
20	10^{11}	$6.30\times10^{+11}$	$6.30\times10^{+11}$	$1.10\times10^{+12}$	$1.10\times10^{+12}$	$1.90\times10^{+06}$	$1.90\times10^{+06}$
30	10^{11}	$6.80\times10^{+11}$	$6.80\times10^{+11}$	$1.20\times10^{+12}$	$1.20\times10^{+12}$	$4.90\times10^{+07}$	$4.90\times10^{+07}$
		Allowed					
1	10^4	$9.40\times10^{+09}$	$9.50\times10^{+09}$	$1.80\times10^{+11}$	$1.80\times10^{+11}$	$5.80\times10^{+09}$	$5.90\times10^{+09}$
5	10^4	$4.70\times10^{+11}$	$4.70\times10^{+11}$	$4.00\times10^{+12}$	$4.00\times10^{+12}$	$5.70\times10^{+09}$	$5.80\times10^{+09}$
10	10^4	$4.70\times10^{+11}$	$4.70\times10^{+11}$	$4.00\times10^{+12}$	$4.00\times10^{+12}$	$5.60\times10^{+09}$	$5.70\times10^{+09}$
20	10^4	$4.70\times10^{+11}$	$4.70\times10^{+11}$	$4.00\times10^{+12}$	$4.00\times10^{+12}$	$5.20\times10^{+09}$	$5.30\times10^{+09}$
30	10^4	$4.60\times10^{+11}$	$4.60\times10^{+11}$	$4.00\times10^{+12}$	$4.00\times10^{+12}$	$4.80\times10^{+09}$	$4.90\times10^{+09}$
1	10^8	$9.30\times10^{+09}$	$9.30\times10^{+09}$	$1.80\times10^{+11}$	$1.80\times10^{+11}$	$4.90\times10^{+09}$	$5.00\times10^{+09}$
5	10^8	$4.70\times10^{+11}$	$4.70\times10^{+11}$	$4.00\times10^{+12}$	$4.00\times10^{+12}$	$5.00\times10^{+09}$	$5.10\times10^{+09}$
10	10^8	$4.70\times10^{+11}$	$4.70\times10^{+11}$	$4.00\times10^{+12}$	$4.00\times10^{+12}$	$5.20\times10^{+09}$	$5.20\times10^{+09}$
20	10^8	$4.70\times10^{+11}$	$4.70\times10^{+11}$	$4.00\times10^{+12}$	$4.00\times10^{+12}$	$5.10\times10^{+09}$	$5.10\times10^{+09}$
30	10^8	$4.60\times10^{+11}$	$4.60\times10^{+11}$	$4.00\times10^{+12}$	$4.00\times10^{+12}$	$4.80\times10^{+09}$	$4.80\times10^{+09}$
1	10^{11}	$8.00\times10^{+00}$	$8.00\times10^{+00}$	$1.20\times10^{+08}$	$1.20\times10^{+08}$	1.40×10^{-57}	1.40×10^{-57}
5	10^{11}	$1.20\times10^{+11}$	$1.20\times10^{+11}$	$1.40\times10^{+12}$	$1.40\times10^{+12}$	1.50×10^{-06}	1.50×10^{-06}
10	10^{11}	$1.20\times10^{+11}$	$1.20\times10^{+11}$	$1.40\times10^{+12}$	$1.40\times10^{+12}$	$2.20\times10^{+01}$	$2.20\times10^{+01}$
20	10^{11}	$1.30\times10^{+11}$	$1.30\times10^{+11}$	$1.50\times10^{+12}$	$1.50\times10^{+12}$	$2.30\times10^{+05}$	$2.30\times10^{+05}$
30	10^{11}	$1.50\times10^{+11}$	$1.50\times10^{+11}$	$1.60\times10^{+12}$	$1.60\times10^{+12}$	$6.80\times10^{+06}$	$6.90\times10^{+06}$

thesis than the BD rates.

Figures 3−8 show that the BD and EC rates increase as the core temperature rises due to a rise in the occupation probability of parent excited states. Consequently, the contribution of the partial rates to the total weak rates becomes significant. The magnitude of the BD rates decreases as the density rises owing to decreased available phase space. The EC rates are enhanced when the electron chemical potential increases with the increase in density.

IV. CONCLUSIONS

The effectiveness of applying the BA hypothesis to calculate the allowed weak rates of heavy nuclei, in general, and forbidden rates, in particular, was missing in the literature. This study investigated the impact of applying the BA hypothesis to calculate the stellar rates. The chosen range of nuclei, having A = 70 – 208 and Z = 27 – 82, has vast applications in the *r*-process nucleosynthesis. The *pn*-QRPA model was employed to evaluate the *Full*

Table 8. Computed total GT strength (ΣB in arbitrary units) and centroid ($\bar{E}$ in MeV units) values for selected nuclei in the EC (left panel) and BD (right panel) directions of the U1F and allowed GT transitions for 10 parent excited states. The energy cutoff in the daughter states is 15 MeV.

EC				BD			
^{86}Kr				^{82}Ge			
$\Sigma B(\mathrm{U1F})_+$	$\Sigma B(\mathrm{GT})_+$	$\bar{E}_+$[U1F]	$\bar{E}_+$[GT]	$\Sigma B(\mathrm{U1F})_-$	$\Sigma B(\mathrm{GT})_-$	$\bar{E}_-$[U1F]	$\bar{E}_-$[GT]
13.95	9.57	3.31	2.24	52.30	49.53	9.09	11.64
41.83	29.66	6.02	5.11	88.73	49.58	24.31	6.00
42.28	28.33	10.00	6.24	158.59	51.28	12.60	6.42
40.74	34.48	7.16	4.50	114.55	49.49	11.20	4.08
42.99	47.55	11.32	5.20	184.16	96.27	11.17	4.67
50.49	48.33	10.81	3.77	551.94	96.41	11.39	6.63
52.75	51.71	12.79	9.41	315.25	126.68	9.40	8.50
38.32	38.16	12.19	9.56	173.40	165.13	12.89	6.07
57.27	31.24	11.35	10.51	227.86	135.00	11.52	3.05
54.70	48.41	12.76	7.86	469.73	148.15	10.87	3.49
^{150}Sm				^{134}Te			
$\Sigma B(\mathrm{U1F})_+$	$\Sigma B(\mathrm{GT})_+$	$\bar{E}_+$[U1F]	$\bar{E}_+$[GT]	$\Sigma B(\mathrm{U1F})_-$	$\Sigma B(\mathrm{GT})_-$	$\bar{E}_-$[U1F]	$\bar{E}_-$[GT]
30.33	17.46	8.56	10.86	249.29	81.30	6.81	8.95
35.89	36.49	8.63	3.66	361.76	318.58	8.78	12.47
37.43	56.22	9.03	6.31	997.63	582.70	8.81	11.31
50.19	62.18	9.14	5.08	1060.19	480.44	8.98	9.08
47.50	41.00	9.49	5.50	1299.62	245.19	13.07	8.81
52.89	67.49	10.07	6.22	3441.34	323.53	10.08	9.84
54.93	62.45	9.58	6.97	1223.27	514.90	10.70	10.01
55.25	55.47	10.84	7.32	1569.68	1621.17	9.45	10.29
67.34	60.42	10.68	7.61	1829.43	1807.52	9.40	10.52
63.47	88.16	11.21	8.57	3165.09	469.26	10.14	10.28
^{207}Tl				^{201}Re			
$\Sigma B(\mathrm{U1F})_+$	$\Sigma B(\mathrm{GT})_+$	$\bar{E}_+$[U1F]	$\bar{E}_+$[GT]	$\Sigma B(\mathrm{U1F})_-$	$\Sigma B(\mathrm{GT})_-$	$\bar{E}_-$[U1F]	$\bar{E}_-$[GT]
29.91	28.72	13.02	12.60	171.66	138.16	11.87	8.57
39.78	27.45	12.92	13.23	205.79	142.55	10.09	8.73
46.08	32.14	13.83	14.20	207.82	137.39	10.12	11.69
3.53	40.29	9.31	11.75	279.69	138.29	9.34	10.84
6.69	43.60	9.93	9.34	172.59	138.23	9.26	12.90
4.80	50.39	9.81	13.17	171.55	138.15	10.91	13.04
7.19	51.26	10.34	11.63	172.55	138.29	12.31	11.75
5.60	53.59	9.70	12.95	172.66	138.13	12.55	13.17
11.22	46.21	9.76	12.40	172.50	137.27	12.53	12.14
3.55	51.44	10.07	12.69	208.95	138.13	11.13	13.24

and BA rates over a wide temperature range (1−30) GK and density (10−10^{11}) g/cm^3 for the allowed GT and U1F rates. The comparison of the microscopic state-to-state calculated rates with those obtained by applying the BA hypothesis indicates a sizeable change in both rate values, particularly for the U1F BD rates. Here, the BA hypothesis is found to have the strongest effect, with deviations exceeding four to five orders of magnitude. Meanwhile, the deviation was rather small for other rates, including the BD and EC rates of the allowed transitions and EC rates of U1F transitions. According to our investigation, the total BA rates (including the allowed and U1F contributions) deviate from the total *Full* rates by an order of magnitude or more. This order of magnitude deviation was recorded for both the EC and BD rates. Core-collapse simulators might find this information useful for modeling purposes. Our findings indicate that the BA hypothesis may be safely applied for BD rates until the core temperature reaches $T = 1$ GK for all density regions. The weak rates based on the BA hypothesis generally begin to deviate from the microscopically calculated rates when the core densities and temperatures exceed 10^4 g/cm^3 and 5 GK, respectively.

Noticeable mentions of the current investigation include:

⊙ For BD rates, a difference of more than one (5) order of magnitude in the allowed (U1F) rates is noted by using BA. Forbidden transitions are more affected by using the BA hypothesis when compared with the allowed GT transitions.

⊙ For small BD rates ($\lambda < 10^{-5}$ s^{-1}), at high core temperatures ($T > 10$ GK) and densities ($\rho Y_e > 10^8$ g/cm^3), a difference of more than five orders of magnitude was reported between the *Full* and BA rates. These temperature-density conditions correspond roughly to the silicon burning phase of the star [73].

⊙ For EC rates, a difference of more than two (1) orders of magnitude in the allowed (U1F) rates is noted by using the BA hypothesis.

⊙ For small EC rates ($\lambda < 10^{-5}$ s^{-1}), at low core temperatures ($T \leq 1$ GK) and densities ($\rho Y_e \leq 10^4$ g/cm^3), a difference of more than 20 orders of magnitude was reported between the *Full* and BA rates. These physical conditions correspond roughly to the C-burning and pre-C-burning phases of the star [73].

⊙ The total BA rates, including the allowed and U1F contributions, deviate by an order of magnitude or more from the total *Full* rates.

These results show that the BA hypothesis significantly impacts the accuracy and reliability of nuclear physics inputs used for *r*-process nucleosynthesis simulations, where the contributions of forbidden transitions to the total rates become large. The current investigation merits due consideration before applying the BA hypothesis to weak rate calculations. In the Appendix, we show the ratios and average deviations of nine new BD and EC nuclei. Detailed data on these and the remaining nuclei may be requested from the corresponding author.

APPENDIX: RATIOS AND AVERAGED RATIOS BETWEEN *Full* AND BA RATES

Comparison of the BA ($\lambda_{\rm BA}$) and *Full* (λ_F) BD rates for three selected nuclei as a function of core temperature (T GK) and density (ρY_e g/cm^3). The ratios (R_i) and average deviation ($\bar{R}$) are given separately for the allowed (All) and forbidden (U1F) transitions, and are defined in Eq. (53) and Eq. (54), respectively. The computed R_i values, where the λ_F and/or $\lambda_{\rm BA}$ rates are less than 10^{-5} s^{-1}, are marked with *. $\bar{R}^{(*)}$ are the computed average deviations excluding ratios marked with *.

Table A1. R_i [All] and R_i [U1F] for three BD nuclei. See text for explanation of symbols.

		^{79}Zn				^{80}Zn				^{96}Zr			
T	ρY_e	R_i [All]		R_i [U1F]		R_i [All]		R_i [U1F]		R_i [All]		R_i [U1F]	
		$\lambda_F \geq \lambda_{\rm BA}$	$\lambda_{\rm BA} > \lambda_F$	$\lambda_F \geq \lambda_{\rm BA}$	$\lambda_{\rm BA} > \lambda_F$	$\lambda_F \geq \lambda_{\rm BA}$	$\lambda_{\rm BA} > \lambda_F$	$\lambda_F \geq \lambda_{\rm BA}$	$\lambda_{\rm BA} > \lambda_F$	$\lambda_F \geq \lambda_{\rm BA}$	$\lambda_{\rm BA} > \lambda_F$	$\lambda_F \geq \lambda_{\rm BA}$	$\lambda_{\rm BA} > \lambda_F$
1	10^4	1.0			1.0		1.0		1.0	1.0$^{(*)}$			1.0$^{(*)}$
10	10^4	1.9			21.6		1.4		11.7	3.7			11272.0
30	10^4	6.6			345.9		3.2		373.3		6.8		158489.3
1	10^8	1.0			6.6		1.0		10.0	2.5$^{(*)}$			2.4$^{(*)}$
10	10^8	2.1			77.8		1.5		32.3	3.3			23173.9
30	10^8	6.6			701.5		3.2		379.3		6.9		130017.0
1	10^{11}	—	—	—	—	—	—	—	—	—	—	—	—
10	10^{11}	6.8$^{(*)}$			15995.6$^{(*)}$		5.0$^{(*)}$		35892.2$^{(*)}$		30.1$^{(*)}$		70957.8$^{(*)}$
30	10^{11}	6.3			31260.8		23.0		67920.4		95.1		65917.4$^{(*)}$
$\bar{\mathbf{R}}$		4.1		6051.4		4.9		13077.5		18.7		57478.9	
$\bar{\mathbf{R}}^{(*)}$		3.7		4630.8		4.9		9818.3		23.2		80738.0	

Table A2. R_i [All] and R_i [U1F] for three BD nuclei. See text for explanation of symbols.

T	$\rho\mathbf{Y_e}$	^{100}Mo				^{124}Sn				^{130}Te			
		R_i [All]		R_i [U1F]		R_i [All]		R_i [U1F]		R_i [All]		R_i [U1F]	
		$\lambda_F \geq \lambda_{BA}$	$\lambda_{BA} > \lambda_F$	$\lambda_F \geq \lambda_{BA}$	$\lambda_{BA} > \lambda_F$	$\lambda_F \geq \lambda_{BA}$	$\lambda_{BA} > \lambda_F$	$\lambda_F \geq \lambda_{BA}$	$\lambda_{BA} > \lambda_F$	$\lambda_F \geq \lambda_{BA}$	$\lambda_{BA} > \lambda_F$	$\lambda_F \geq \lambda_{BA}$	$\lambda_{BA} > \lambda_F$
1	10^4	4.7$^{(*)}$			1.0$^{(*)}$	1.0			1.0	146.6$^{(*)}$		12.3$^{(*)}$	
10	10^4	3.6			2041.7$^{(*)}$	38.2			76.2	41.2			25.5
30	10^4		7.8		56623.9	11.4			1419.1	16.6			8953.6
1	10^8	5.7$^{(*)}$			33.3$^{(*)}$	1.0			1.0	263.6$^{(*)}$		8.2$^{(*)}$	
10	10^8	3.3			1798.9$^{(*)}$	40.0			1205.0	38.5			28119.0$^{(*)}$
30	10^8		7.9		58479.0	11.4			9311.1	16.6			85113.8
1	10^{11}	—	—	—	—	—	—	—	—	—	—	—	—
10	10^{11}		28.3$^{(*)}$		14060.5$^{(*)}$	14.7$^{(*)}$			47643.1$^{(*)}$	20.4$^{(*)}$			54075.4$^{(*)}$
30	10^{11}		98.9		240990.5$^{(*)}$	10.9			36728.2	13.6			67764.2
$\bar{\mathbf{R}}$		20.0		46753.6		16.1		12048.1		69.6		30509.0	
$\bar{\mathbf{R}}^{(*)}$		24.3		57551.5		16.3		6963.1		25.3		40464.3	

Table A3. R_i [All] and R_i [U1F] for three BD nuclei. See text for explanation of symbols.

T	$\rho\mathbf{Y_e}$	^{136}Xe				^{150}Nd				^{202}Os			
		R_i [All]		R_i [U1F]		R_i [All]		R_i [U1F]		R_i [All]		R_i [U1F]	
		$\lambda_F \geq \lambda_{BA}$	$\lambda_{BA} > \lambda_F$	$\lambda_F \geq \lambda_{BA}$	$\lambda_{BA} > \lambda_F$	$\lambda_F \geq \lambda_{BA}$	$\lambda_{BA} > \lambda_F$	$\lambda_F \geq \lambda_{BA}$	$\lambda_{BA} > \lambda_F$	$\lambda_F \geq \lambda_{BA}$	$\lambda_{BA} > \lambda_F$	$\lambda_F \geq \lambda_{BA}$	$\lambda_{BA} > \lambda_F$
1	10^4	133.0$^{(*)}$			7.2$^{(*)}$	9.0$^{(*)}$			1.0$^{(*)}$	1.0			1.0
10	10^4	46.7			13091.8	2.4			251.2$^{(*)}$	21.9			1472.3
30	10^4	28.7			130017.0		1.6		20844.9	19.3			2454.7
1	10^8	150.0$^{(*)}$			1.2$^{(*)}$	11.5$^{(*)}$			1.0$^{(*)}$	1.0$^{(*)}$			1.0$^{(*)}$
10	10^8	44.3			8260.4	2.0			7620.8$^{(*)}$	22.3			26977.40
30	10^8	28.6			314050.9		1.7		135831.3	19.3			62517.3
1	10^{11}	—	—	—	—	—	—	—	—	—	—	—	—
10	10^{11}	29.9$^{(*)}$			68706.8$^{(*)}$		3.2 $^{(*)}$		33728.7$^{(*)}$	19.1$^{(*)}$			16943.4$^{(*)}$
30	10^{11}	26.5			135207.3$^{(*)}$		2.8		113501.1$^{(*)}$	19.1			344349.9$^{(*)}$
$\bar{\mathbf{R}}$		61.0		83667.8		4.3		38972.5		15.4		56839.6	
$\bar{\mathbf{R}}^{(*)}$		35.0		116355.0		2.1		78338.1		17.1		18684.5	

Table A4. R_i [All] and R_i [U1F] for three EC nuclei. See text for explanation of symbols.

T	$\rho\mathbf{Y_e}$	^{76}Ge				^{76}Se				^{82}Se			
		R_i [All]		R_i [U1F]		R_i [All]		R_i [U1F]		R_i [All]		R_i [U1F]	
		$\lambda_F \geq \lambda_{BA}$	$\lambda_{BA} > \lambda_F$	$\lambda_F \geq \lambda_{BA}$	$\lambda_{BA} > \lambda_F$	$\lambda_F \geq \lambda_{BA}$	$\lambda_{BA} > \lambda_F$	$\lambda_F \geq \lambda_{BA}$	$\lambda_{BA} > \lambda_F$	$\lambda_F \geq \lambda_{BA}$	$\lambda_{BA} > \lambda_F$	$\lambda_F \geq \lambda_{BA}$	$\lambda_{BA} > \lambda_F$
1	10^4	77.6$^{(*)}$			1.6$^{(*)}$	1.0$^{(*)}$			1.0$^{(*)}$	66069.3$^{(*)}$			1.9$^{(*)}$
10	10^4		1.5		1.9	2.9			1.1		1.9		2.1
30	10^4	3.8		4.0		5.5		4.5		4.0		4.3	
1	10^8	69.5$^{(*)}$			1.5$^{(*)}$	1.0$^{(*)}$		1.0$^{(*)}$		64416.9$^{(*)}$			1.9$^{(*)}$
10	10^8		1.5		1.9	2.9			1.1		1.9		2.1
30	10^8	3.8		4.0		5.5		4.5		4.0		4.3	

Continued on next page

Table A4-continued from previous page

T	$\rho\mathbf{Y_e}$	^{76}Ge				^{76}Se				^{82}Se			
		R_i [All]		R_i [U1F]		R_i [All]		R_i [U1F]		R_i [All]		R_i [U1F]	
		$\lambda_F \geq \lambda_{BA}$	$\lambda_{BA} > \lambda_F$	$\lambda_F \geq \lambda_{BA}$	$\lambda_{BA} > \lambda_F$	$\lambda_F \geq \lambda_{BA}$	$\lambda_{BA} > \lambda_F$	$\lambda_F \geq \lambda_{BA}$	$\lambda_{BA} > \lambda_F$	$\lambda_F \geq \lambda_{BA}$	$\lambda_{BA} > \lambda_F$	$\lambda_F \geq \lambda_{BA}$	$\lambda_{BA} > \lambda_F$
1	10^{11}	1.0		1.0		1.0		1.0		1.0		1.0	
10	10^{11}	1.4		1.4		1.5		1.4		1.4		1.4	
30	10^{11}	7.7		6.5		8.8		6.7		8.2		7.2	
$\bar{\mathbf{R}}$		18.7		2.6		3.3		2.5		14501.0		2.9	
$\bar{\mathbf{R}}^{(*)}$		3.0		3.0		4.0		2.9		3.2		3.2	

Table A5. R_i [All] and R_i [U1F] for three EC nuclei. See text for explanation of symbols.

T	$\rho\mathbf{Y_e}$	^{88}Sr				^{90}Zr				^{128}Te			
		R_i [All]		R_i [U1F]		R_i [All]		R_i [U1F]		R_i [All]		R_i [U1F]	
		$\lambda_F \geq \lambda_{BA}$	$\lambda_{BA} > \lambda_F$	$\lambda_F \geq \lambda_{BA}$	$\lambda_{BA} > \lambda_F$	$\lambda_F \geq \lambda_{BA}$	$\lambda_{BA} > \lambda_F$	$\lambda_F \geq \lambda_{BA}$	$\lambda_{BA} > \lambda_F$	$\lambda_F \geq \lambda_{BA}$	$\lambda_{BA} > \lambda_F$	$\lambda_F \geq \lambda_{BA}$	$\lambda_{BA} > \lambda_F$
1	10^4	$1.9\times10^{+09(*)}$			$1.5^{(*)}$	$274789.4^{(*)}$			$1.0^{(*)}$	$1517.1^{(*)}$			$1.5^{(*)}$
10	10^4	10.0			1.8	74.1			1.1	6.6		1.2	
30	10^4	6.7		3.9		55.0		7.1		6.1		7.7	
1	10^8	$1.7\times10^{+09(*)}$			$1.5^{(*)}$	$1.1^{(*)}$		$1.0^{(*)}$		$95.1^{(*)}$			$1.3^{(*)}$
10	10^8	9.9			1.8	70.6			1.1	6.6		1.2	
30	10^8	6.7		3.9		55.0		7.1		6.1		7.7	
1	10^{11}	1.0		1.0		1.0		1.0		1.0		1.0	
10	10^{11}	1.8		1.3		5.4		1.3		3.0		2.9	
30	10^{11}	9.8		5.3		53.8		9.3		12.4		12.6	
$\bar{\mathbf{R}}$		$4.0\times10^{+08}$		2.4		30567.3		3.3		183.8		4.1	
$\bar{\mathbf{R}}^{(*)}$		6.6		2.7		45.0		4.0		6.0		4.9	

Table A6. R_i [All] and R_i [U1F] for three EC nuclei. See text for explanation of symbols.

T	$\rho\mathbf{Y_e}$	^{186}Nd				^{195}Tm				^{204}Pt			
		R_i [All]		R_i [U1F]		R_i [All]		R_i [U1F]		R_i [All]		R_i [U1F]	
		$\lambda_F \geq \lambda_{BA}$	$\lambda_{BA} > \lambda_F$	$\lambda_F \geq \lambda_{BA}$	$\lambda_{BA} > \lambda_F$	$\lambda_F \geq \lambda_{BA}$	$\lambda_{BA} > \lambda_F$	$\lambda_F \geq \lambda_{BA}$	$\lambda_{BA} > \lambda_F$	$\lambda_F \geq \lambda_{BA}$	$\lambda_{BA} > \lambda_F$	$\lambda_F \geq> \lambda_{BA}$	$\lambda_{BA} > \lambda_F$
1	10^4	—	—	—	—	$1.1\times10^{+06(*)}$			$12.0^{(*)}$	$31.8^{(*)}$			$8.5^{(*)}$
10	10^4	$55.7^{(*)}$			$5.1^{(*)}$		1.3	1.2			1.6		3.5
30	10^4	14.9		2.6		15.4		12.1		3.3		3.7	
1	10^8	—	—	—	—	$1.1\times10^{+06(*)}$			$12.0^{(*)}$	$31.8^{(*)}$			$8.6^{(*)}$
10	10^8	$55.7^{(*)}$			$5.1^{(*)}$		1.3	1.2			1.6		3.5
30	10^8	14.9		2.6		15.4		12.1		3.3		3.7	
1	10^{11}	$1.0^{(*)}$		$1.0^{(*)}$		1.1		1.1		1.0		1.0	
10	10^{11}	50.4			2.9	5.5		4.2		2.0		2.0	
30	10^{11}	14.4		2.7		26.2		15.8		5.2		5.2	
$\bar{\mathbf{R}}$		29.6		3.2		$2.4\times10^{+05}$		8.0		9.1		4.4	
$\bar{\mathbf{R}}^{(*)}$		23.6		2.7		9.5		6.8		2.6		3.2	

References

[1] H. Homma, E. Bender, M. Hirsch M *et al*., Phys. Rev. C **54**, 2972 (1996)
[2] P. Möller, B. Pfeiffer, and K-L Kratz, Phys. Rev. C **67**, 055802 (2003)
[3] Q. Zhi, E. Caurier, J. J. Cuenca-García *et al*., Phys. Rev. C **87**, 025803 (2013)
[4] J.-U. Nabi and S. Stoica, Astrophys. Space. Sci **349**, 843 (2014)
[5] T. Suzuki, M. Honma, T. Yoshida *et al*., Prog. Part. Nucl. Phys. **66**, 385 (2011)
[6] J.-U. Nabi, N. Çakmak, S. Stoica *et al*., Phys. Scr. **90**, 115301 (2015)
[7] J.-U. Nabi and H. V. Klapdor-Kleingrothaus, At. Data Nucl. Data Tables **88**, 237 (2004)
[8] D. D. Clayton, *Principles of Stellar Evolution and Nucleosynthesis* (New York: McGraw-Hill, 1968)
[9] E. M. Ney, J. Engel, T. Li *et al*., Phys. Rev. C **102**, 034326 (2020)
[10] J. J. Cowan, C. Sneden, J. E. Lawler *et al*., Rev. Mod. Phys. **93**, 015002 (2021)
[11] C. J. Horowitz *et al*., J. Phys. G: Nucl. Part. Phys. **46**, 083001 (2019)
[12] J.-U. Nabi, A. Ullah, S.A.A. Shah *et al*., Act. Phys. Pol. B **50**, 1523 (2019)
[13] J.-U. Nabi, T. Bayram, G. Daraz *et al*., Nucl. Phys. A **1015**, 122278 (2021)
[14] J.-U. Nabi, N. Çakmak, A. Ullah *et al*., Phys. Scr. **96**, 115303 (2021)
[15] T. Marketin, L. Huther, and G. Martínez-Pinedo, Phys. Rev. C **93**, 025805 (2016)
[16] I. N. Borzov, J. J. Cuenca-García, K. Langanke *et al*., Nucl. Phys. A **814**, 159 (2008),
[17] D. Watson *et al*., Nature **574**, 497 (2019)
[18] J. H. Thies, D. Frekers, T. Adachi *et al*., Phys. Rev. C **86**, 014304 (2012)
[19] D. Frekers and M. Alanssari, Eur. Phys. J. A **54**, 177 (2018)
[20] P. Puppe, A. Lennarz, T. Adachi *et al*., Phys. Rev. C **86**, 044603 (2012)
[21] J. Yasuda *et al*., Phys. Rev. Lett. **121**, 132501 (2018)
[22] C. J. Guess *et al*., Phys. Rev. C **83**, 064318 (2011)
[23] T. Wakasa *et al*., Phys. Rev. C **85**, 064606 (2012)
[24] K, Langanke and G. Martínez-Pinedon, Nucl. Phys. A **673**, 481 (2000)
[25] S. Nishimura *et al*., Phys. Rev. Lett. **106**, 052502 (2011)
[26] G. Lorusso *et al*., Phys. Rev. Lett **114**(19), 192501 (2015)
[27] A. C. Dombos *et al*., Phys. Rev. C **99**(1), 015802 (2019)
[28] J. Liang *et al*., Nucl. Data Sheets **168**, 1 (2020)
[29] O. Hall *et al*., Physics Letters B **816**, 136266 (2021)
[30] G. M. Fuller, W. A. Fowler, and M. J. Newman, Astrophys. J. **252**, 715 (1982)
[31] M. B. Aufderheide, I. Fushiki, and S. E. Woosley *et al*., Astrophys. J. Suppl. **91**, 389 (1994)
[32] K. Langanke and G. Martínez-Pinedon, Rev. Mod. Phys. **75**, 819 (2003)
[33] A. Cole, T. Anderson, R. Zegers *et al*., Phys. Rev. C **86**, 015809 (2012)
[34] D.M. Brink, D. Phil. thesis (unpublished), (Oxford University UK, 1955)
[35] P. Axel, Phys. Rev. **126**, 671 (1962)
[36] C. W. Johnson, Phys. Lett. B **750**, 72 (2015)
[37] Y. Lu and C. W. Johnson, Phys. Rev. C **97**, 034330 (2018)
[38] C. T. Angell, S. L. Hammond, H. J. Karwowski *et al*., Phys. Rev. C **86**, 051302 (2012)
[39] A. C. Larsen *et al*., Phys. Rev. C **76**, 044303 (2007)
[40] N. Frazier, B. A. Brown, D. Millener *et al*., Phys. Lett. B **414**, 7 (1997)
[41] G. W. Misch, G. M. Fuller, and B. A. Brown, Phys. Rev. C **90**, 065808 (2014)
[42] J.-U. Nabi and M.-U. Rahman, Phys.Rev. C **75**, 035803 (2007)
[43] J.-U. Nabi and M. Riaz, J. Phys. G: Nucl. Part. Phys. **46**, 085201 (2019)
[44] E. Yüksel, N. Paar, G. Colò *et al*., Phys. Rev. C **101**, 044305 (2020)
[45] R. A. Herrera, C. W. Johnson, and G. M. Fuller, Phys. Rev. C **105**, 015801 (2022)
[46] J.-U. Nabi, M. Nayab, and C..W. Johnson, J. Phys. G: Nucl. Part. Phys. **49**, 065201 (2022)
[47] F. Farooq, J.-U. Nabi, and R. Shehzadi, Phys. Scr. **98**, 085313 (2023)
[48] B. Pfeiffer, K.-L. Kratz, and P. Möller, Prog. Nucl. Energy **41**, 39 (2002)
[49] J. J. Cuenca-García, G. Martínez-Pinedo, K. Langanke *et al*., Eur. Phys. J. A **34**, 99 (2007)
[50] I. N. Borzov, Phys. Rev. C **67**, 025802 (2003
[51] Y. Zhou *et al*., Sci. China Phys. Mech. Astron. **60**, 082012 (2017)
[52] Z. M. Niu, H. Z. Liang, B. H. Sun *et al*., Phys. Rev. C **99**, 064307 (2019)
[53] M. Hirsch, A. Staudt, K. Muto *et al*., At. Data Nucl. Data Tables **53**, 165 (1993)
[54] A. Staudt, E. Bender, K. Muto *et al*., At. Data Nucl. Data Tables **44**, 79 (1990)
[55] C. Robin, E. Litvinova, and G. Martínez-Pinedo, EPJ Web of Conferences **260**, 03002 (2022)
[56] J.-U. Nabi, N. Çakmak, and Z. Iftikhar, Eur. Phys. J. A **52**(1), 1 (2016)
[57] F. Farooq, J.-U. Nabi, and R. Shehzadi, Phys. Scr. **96**, 125312 (2021)
[58] V. A. Kuz-Min and V. G. Soloviev, Nucl. Phys. A **486**, 118 (1988)
[59] J. A. Halbleib Sr and R. A. Sorensen, Nucl. Phys. A **98**, 542 (1967)
[60] K. Muto, E. Bender, T. Oda *et al*., Z. Phys. A **341**, 407 (1992)
[61] P. Möller and J. Randrup, Nucl. Phys. A **514**, 1 (1990)
[62] E. Bender, K. Muto, and H.V. Klapdor-Kleingrothaus, Phys. Lett. B **208**, 53 (1988)
[63] K. Muto, E. Bender, and H.V. Klapdor-Kleingrothaus, Z. Phys. A **333**, 125 (1989)
[64] S. G. Nilsson, Mat. Fys. Medd. Dan. Vid. Selsk **29**, 1 (1955)
[65] M. Wang, G. Audi, A.H. Wapstra, *et al*., Chin. Phys. C **36**, 1603 (2012)
[66] P. Möller, M.R. Mumpower, T. Kawano, *et al*., At. Data Nucl. Data Tables **125**, 1 (2019)
[67] https://www-nds.iaea.org/relnsd/vcharthtml/VChartHTML.html
[68] P. Möller, A.J. Sierk, T. Ichikawa *et al*., At. Data Nucl. Data Tables **109**, 1 (2016)
[69] N.B. Gove and M.J. Martin, At. Data Nucl. Data Tables **10**, 205 (1971)
[70] K. Nakamura *et al*. (Particle Data Group), J. Phys. G: Nucl. Part. Phys. **37**(7), 075021 (2010)
[71] B. Gao *et al*., Phys. Rev. C **101**, 014308 (2020)
[72] R. L. Helmer *et al*., Phys. Rev. C **55**, 2802 (1997)
[73] N. Prantzos and S. Ekström *Stellar Nucleosynthesis* (In: Gargaud, M., *et al*. Encyclopedia of Astrobiology. Springer, Berlin, Heidelberg, 2011)